

February 2020

Mechanisms of Carbon Movement and Stabilization in Mangrove Wetlands

Carey Schafer
University of South Florida

Follow this and additional works at: <https://digitalcommons.usf.edu/etd>



Part of the [Biogeochemistry Commons](#), [Geology Commons](#), and the [Soil Science Commons](#)

Scholar Commons Citation

Schafer, Carey, "Mechanisms of Carbon Movement and Stabilization in Mangrove Wetlands" (2020). *USF Tampa Graduate Theses and Dissertations*.
<https://digitalcommons.usf.edu/etd/8990>

This Thesis is brought to you for free and open access by the USF Graduate Theses and Dissertations at Digital Commons @ University of South Florida. It has been accepted for inclusion in USF Tampa Graduate Theses and Dissertations by an authorized administrator of Digital Commons @ University of South Florida. For more information, please contact digitalcommons@usf.edu.

Mechanisms of Carbon Movement and Stabilization in Mangrove Wetlands

by

Carey Schafer

A thesis submitted in partial fulfillment
of the requirements for the degree of
Master of Science in Marine Science
with a concentration in Geological Oceanography
College of Marine Science
University of South Florida

Major Professor: Brad Rosenheim, Ph.D.
Joseph M. Smoak, Ph.D.
Christopher Smith, Ph.D.

Date of Approval:
February 28, 2020

Keywords: blue carbon, Ten Thousand Islands, Ramped PyrOx, root exudates, activation energy
distributions

Copyright © 2020, Carey Schafer

Acknowledgments

First off, I would like to thank my advisor Dr. Brad Rosenheim for his support throughout my graduate (and one semester of my undergraduate) career. Thank you for not only allowing me to foster a love for science but for encouraging me to pursue passions related to science outreach and education. I would also like to my lab mates, Ryan, Theresa, and Dylan, who have provided me with endless help and encouragement both in and out of the lab. My time at CMS would have not been the same without you all. I would like to thank Dr. Joseph Smoak at USFSP and Dr. Christopher Smith at USGS for serving on my committee and providing me with guidance and feedback throughout my graduate career. In addition, I would like to thank Dr. Joseph Smoak and Amanda Chappell for developing ^{210}Pb chronologies at USFSP and Dr. Thomas Bianchi and Dr. Derrick Vaughn for analyzing lignin data at the University of Florida. This project would have not been possible without the many hours of field work led by Dr. Ryan Moyer and Dr. Kara Radabaugh. Thank you to Jon Sharp who helped with statistics and coding in MatLab and remained patient in the face of my frustration. I would also like to thank the USDA, the Paul Getting Endowed Fellowship in Marine Science and the St. Petersburg Downtown Partnership in Coastal Science for supporting me financially. Finally, I would like to thank my family and friends for their endless encouragement. I would not be where I am today without your support.

Table of Contents

List of Tables	iii
List of Figures.....	iv
Abstract	vi
Chapter One: Introduction	1
1.1 Research Questions.....	8
Chapter Two: Methods	9
2.1 Study Site and Core Collection.....	9
2.2 Soil Composition	10
Loss on Ignition	10
Elemental Analysis	10
Lignin Content	11
2.3 Chronometers.....	12
Lead-210 and Cesium-137.....	12
Radiocarbon (¹⁴ C).....	12
Radiocarbon Sample Preparation.....	12
Ramped PyrOx.....	14
Bulk Combustion	14
Blank Correction.....	15
2.4 Data Analysis.....	16
Activation Energy Distributions – rampedpyrox Python Package	16
Turnover Time	17
Chapter Three: Mangrove Carbon Storage Efficiency Facilitated by Young Carbon Transport.....	21
Chapter Four: Conclusions	33
References	35
Appendix A: Supplementary Information for Chapter Three.....	40
A.1 Carbon Burial Calculations.....	41
A.2 Alternative Carbon Transport Mechanisms	42
Bioturbation	42
Root Hairs	42
Humic Acids	43

Tidal Flushing	44
Interstitial Carbonate Dissolution	45
A.3 Evidence for a Single-Pool Turnover Model	45
Appendix B: The Influence of Root Hairs on the Isotopic Composition of Soil Organic	47
B.1 Motivation	47
B.2 Methods	47
B.3 Results and Discussion.....	48
B.4 Conclusions	50
Appendix C: The Impact of Grain Size on Bulk Soil Organic Matter Radiocarbon	
Content.....	53
C.1 Motivation	53
C.2 Methods.....	53
C.3 Results and Discussion.....	53
C.4 Conclusions	56
Appendix D: Description of Accretion Calculations and Timescale Bias in Ten	
Thousand Islands, Florida.....	57
D.1 Motivation	57
D.2 Methods.....	57
D.3 Results and Discussion.....	58
D.4 Conclusions.....	62
Appendix E: Radiocarbon and Stable Isotopic Data.....	63

List of Tables

Table 1: Modern and dead blank values for Ramped PyrOx and bulk combustion	16
Table 2: Input variables, input error, output variables, and output error for the Monte Carlo simulation.....	17
Table 1A: Two end-member mixing model for the open mangrove (OM) site. Used to determine the mass of young carbon buried at each site	41
Table 2A: Two end-member mixing model for the confined mangrove (CM) site. Used to determine the mass of young carbon buried at each site	41
Table 1B: Root hair radiocarbon content (fraction modern, Fm) divided by size class, and the corresponding stable isotopic signatures ($\delta^{13}\text{C}$) and ^{210}Pb ages for the open (M_{O}) and confined (M_{C}) mangrove sites.....	50
Table 2B: Unsieved bulk soil organic matter radiocarbon content (fraction modern, Fm), and corresponding stable carbon isotopic signatures ($\delta^{13}\text{C}$) and ^{210}Pb ages for the open (M_{O}) and confined (M_{C}) mangrove sites.....	51
Table 3B: Elemental analysis data (%N, %C, and C:N ratios) from two intervals at the open mangrove (M_{O}) and confined mangrove (M_{C}) sites.....	52
Table 1C: Peak ^{14}C values for the open mangrove (M_{O}) and confined mangrove (M_{C}) sites divided by grain size.....	55
Table 1D: Accretion rates (cm/yr) for the open mangrove (M_{O}) and confined mangrove (M_{C}) sites based on the depths of ^{137}Cs peaks	59
Table 1E: Radiocarbon (^{14}C) and stable carbon isotopic ($\delta^{13}\text{C}$) data for the open mangrove site.....	63
Table 2E: Radiocarbon (^{14}C) and stable carbon isotopic ($\delta^{13}\text{C}$) data for the confined mangrove site.....	66

List of Figures

Figure 1: Schematic of Northern Hemisphere Bomb spike and soil turnover times.....	4
Figure 2: Image of an unsieved sample from the confined mangrove site.....	10
Figure 3: Schematic of filtration apparatus	13
Figure 4: Cumulative carbon plots for open and confined mangrove sites.....	19
Figure 5: Probability distributions for input (I) and decomposition (k) values for the open and confined mangrove sites.....	20
Figure 6: Map of study sites in Ten Thousand Islands, Florida, USA	23
Figure 7: Radiocarbon (^{14}C) results from the open and confined mangrove sites in Ten Thousand Islands, Florida.....	25
Figure 8: Downcore profiles of ^{210}Pb and ^{137}Cs	26
Figure 9: Downcore activation energy distributions and $(\text{Ad}/\text{Al})_v$ profiles from the open and confined mangrove sites.....	30
Figure 10: Conceptual diagram explaining soil organic carbon (SOC) cycling and stabilization at the open and confined mangrove sites.....	31
Figure 1A: Comparison of radiocarbon values (fraction modern, F_m) from Ramped PyrOx and bulk combustion from the open mangrove site.....	40
Figure 2A: Radiocarbon (^{14}C) values from unsieved material and root hairs indicate root hairs were not the source of young carbon at depth	42
Figure 3A: Comparison of radiocarbon (^{14}C) values from acid-base-acid (ABA) treated samples, sieved and unsieved samples indicates humic acids did not bias dates to be younger	43
Figure 4A: C:N ratios and $\delta^{13}\text{C}$ values of sieved material from the open mangrove and confined mangrove sites show no influence of marine organic matter.	44
Figure 5A: Thermographs from Ramped PyrOx analysis	45

Figure 1B: Radiocarbon (fraction modern, Fm) values of large and small root hairs for The open mangrove (OM) and confined mangrove (CM) sites.....	48
Figure 2B: Downcore comparison of stable carbon isotopic data ($\delta^{13}\text{C}$) for bulk soil and root hairs	49
Figure 1C: Radiocarbon (fraction modern, Fm) values for sieved and unsieved organic matter from the open mangrove and confined mangrove sites	54
Figure 2C: C:N ratios and stable carbon isotopic data ($\delta^{13}\text{C}$) for sieved and unsieved material from the open and confined mangrove sites	54
Figure 1D: Accretion rates (cm/yr) for Ten Thousand Islands, Florida based on ^{137}Cs , ^{210}Pb , and ^{14}C chronologies.....	58
Figure 2D: Ten Thousand Islands accretion rates (cm/yr) from combined open mangrove and confined mangrove ^{210}Pb and ^{14}C records.....	59
Figure 3D: Conceptual diagram describing accretion modeling	60
Figure 4D: Modeled accretion rates (cm/yr) for the open mangrove site.....	61

Abstract

Mangrove forests have higher rates of carbon storage per unit area than any other coastal or terrestrial habitat, largely due to their significant soil stocks. More effort has been placed on quantifying mangrove soil carbon stock, the amount of carbon stored in the upper meter of mangrove soils, than identifying the processes governing *in situ* soil organic carbon (SOC) cycling and stabilization. An understanding of the mechanisms related to carbon transport and stability is necessary to constrain current wetland carbon stocks and to determine how sea level rise will impact future carbon stores. This study uses a variety of radiometric chronometers (^{210}Pb , ^{137}Cs , and ^{14}C) paired with stable carbon isotopes, elemental analysis, downcore lignin profiles, and activation energy distributions to provide insight into mangrove SOC dynamics. Using these methods, I have identified a transport mechanism whereby young carbon is advected downward in pore waters and stabilized in the particulate form. I estimate over the last 120 years, the downward advection of carbon has led to the storage of 184 Tg of carbon in mangrove soils globally. In addition, I investigated the source of young carbon and the influence source played in long-term SOC stability. My data suggest young carbon is sourced from root exudates which are transported in pore waters and stabilized through microbially processing. Calculations of turnover time revealed differences in the timescale of carbon storage between sites that varied in tidal influence, with a longer turnover time at a site with inundated soils, but minimal tidal influence. This suggests inundation serves to enhance stability but is not the ultimate mechanism governing mangrove SOC stability.

Chapter 1. Introduction

Coastal marine ecosystems are widely recognized for their carbon storage capacity (McLeod et al., 2011). In the most recent report from the Intergovernmental Panel on Climate Change (IPCC), scientists emphasized the negative consequences of higher CO₂ emissions, including rising sea levels and global temperatures (Allen et al., 2018). For this reason, the IPCC has stressed the need to not only reduce emissions, but also capture CO₂ from the atmosphere (Allen et al., 2018). As a result, coastal ecosystems are now looked to as a natural and effective way to curb increased CO₂ emissions (Canadell and Raupach, 2008). These “blue carbon” sinks include mangrove forests, seagrass beds, and salt marshes. Although they comprise a small proportion of coastal land area, these habitats are acknowledged as one of the largest components of the terrestrial biological carbon pool (Dixon and Krankina, 1995; McLeod et al., 2011). Mangroves, specifically, cover only 0.5% of coastal land area globally, yet have the highest rate of carbon storage per unit area among vegetated ecosystems, including tidal marshes, seagrasses, and evergreen forests (Alongi, 2014).

As the Earth continues to warm, the latitudinal range in which mangroves can survive is expanding due to less frequent and intense frost events (Saintilan et al., 2014). In addition, sea level rise (SLR) has resulted in the landward encroachment of mangrove forests, further increasing the extent of their habitat (Krauss et al., 2011). Areas previously occupied by marshes are now inhabited by mangroves, leading to a net increase in carbon storage due to an increase in aboveground biomass and the upward accretion of peat (Donato et al., 2011; Doughty et al., 2016; Simpson et al., 2017; Yao & Liu, 2017). However, the ability of mangrove ecosystems to cope

with SLR may be diminished as droughts and hurricanes are exacerbated by climate change (Jones et al., 2019). Systems damaged by these climatic events have been unable to keep up with SLR in the past, resulting in the loss of soil carbon through marine transgressions (Jones et al., 2019).

The main objective of this thesis is to examine soil organic carbon (SOC) cycling and stability in mangrove soils. Blue carbon research has largely focused on quantifying global mangrove soil carbon stock and the fluxes of carbon in and out of these systems (Bouillon et al., 2008; Breithaupt et al., 2012; Chmura et al., 2003; Donato et al., 2011; Duarte and Cebrián, 1996; Kristensen et al., 2008). However, less effort has been put into identifying and quantifying the mechanisms controlling SOC movement and stabilization in mangrove habitats. A greater understanding of these processes will help to refine current stock estimates and determine how mangrove carbon stocks will respond to future changes in climate.

Establishing the fluxes of carbon into and out of mangrove ecosystems is vital to understanding carbon cycling within mangrove soils. Carbon inputs can be divided into two broad categories: carbon that is produced elsewhere and brought in via tidal flow (allochthonous carbon) and carbon that is produced from the breakdown of mangrove material (autochthonous carbon). It has been estimated that allochthonous inputs to mangrove soils are 10 Tg C yr⁻¹ (Alongi, 2014). Allochthonous carbon inputs include particulate organic carbon (POC) and dissolved organic carbon (DOC). These inputs bear a marine $\delta^{13}\text{C}$ signature, derived from sources such as phytoplankton or seagrasses (Kristensen et al., 2008). Allochthonous inputs also include inorganic carbon, such as carbonate minerals, that are sourced from marine settings (Woodroffe et al., 2016). Mangrove net primary production is 210 Tg C yr⁻¹ and represents autochthonous carbon inputs. More than one-third of net primary production is the result of fine root production, while wood production and litter fall constitute the remaining two-thirds of primary productivity (Alongi,

2014). Although the sources of autochthonous carbon have been identified and quantified, the fate of mangrove primary production is much less understood. More than 50% of mangrove primary production ($\sim 104 \pm 86.5 \text{ Tg C a}^{-1}$) is unaccounted for in current blue carbon budgets (Breithaupt et al., 2012). Recent research has suggested this missing carbon is the result of dissolved inorganic carbon export (Maher et al., 2013).

Mangrove photosynthetic production is exported from the system as either dissolved inorganic carbon (DIC), gas (CO_2 or CH_4), DOC, or leaf litter and other suspended solids (POC) (Duarte and Cebrián, 1996). Maher et al. (2013) suggested the unaccounted carbon in net primary productivity budgets was exported as DIC through tidally driven advective porewater flux, making DIC the dominant form of carbon exported from mangroves. Soil CO_2 flux is the result of mainly aerobic microbes and anaerobic sulfate reducers, while factors such as increased soil temperature can serve to enhance CO_2 effluxes (Kristensen et al., 2008; Lewis et al., 2014). Sulfate reduction decreases the concentrations of hydrogen and acetate, largely limiting methanogens and the production of methane within mangrove soils (Alongi, 2014; Kristensen et al., 2008). DOC, produced through the leaching and decomposition of organic material, along with POC are transported from the system via tidal and groundwater flow.

About 10% of mangrove primary production is ultimately buried in sediments, accounting for 15% of carbon storage along coasts (Alongi, 2014; Duarte and Cebrián, 1996). Globally, this results in an annual burial rate of $26.1 \pm 5.7 \text{ Tg OC yr}^{-1}$ (Alongi, 2014; Breithaupt et al., 2012). Whereas nearly constant tidal flushing serves as a pathway for carbon export, tidal inundation protects peat from aerobic microbial mineralization and meiofaunal heterotrophy, making it stable *in situ*. These conditions create anoxic environments that slow the degradation of cellulose and

lignin and allow for the accumulation of vast stocks of carbon (Alongi, 2014; Donato et al., 2011; Kristensen et al., 2008; Lewis et al., 2014).

The calculation of soil turnover time (τ) provides a way to quantify the timescale of SOC storage and is defined as the ratio of total carbon stock at a defined depth to an input or output flux (Sierra et al., 2017). In general, soils are often modeled as multiple active pools of carbon which turnover at different rates, ranging from years (e.g. undecomposed litter) to thousands of years (e.g. mineral-bound carbon)

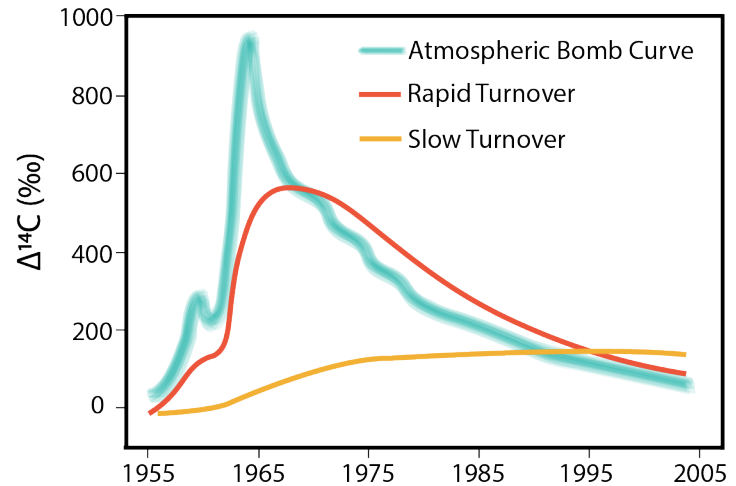


Figure 1 Schematic of Northern Hemisphere Bomb spike and soil turnover times. Northern Hemisphere radiocarbon bomb curve and two soil bomb curves with varying turnover times. A slow turnover time corresponds to a slower exchange of carbon between the soil and the atmosphere, resulting in an elongated shape. Adapted from Torn et al. (2009).

(Jenkinson & Rayner, 1977; Townsend et al., 1995; Trumbore, 2000, 2009; Trumbore et al., 1989).

Upland terrestrial ecosystems have largely been the focus of SOC turnover studies. As a result, it is unclear whether a single or multi-pool model more appropriately represents the SOC dynamics in wetlands. Yet, better constraining wetland turnover is vital for determining the timescale of carbon storage.

Laboratory and field-based experiments, utilizing radiocarbon (^{14}C) produced from nuclear fallout, provide one way to validate modeled SOC turnover. Nuclear weapons testing in the 1960s nearly doubled the amount of naturally-occurring atmospheric ^{14}C present in the Northern Hemisphere. Since the initial spike of this so-called “bomb radiocarbon”, the amount of atmospheric ^{14}C has decreased exponentially as it has been incorporated into marine and terrestrial

carbon pools (Trumbore, 2009). Soil turnover times can be calculated based on the amount of bomb ^{14}C present in a soil sample, which gives insight into the flux of carbon between the atmosphere and the soil (Figure 1) (Trumbore, 2009). Traditionally, physical and chemical fractionation have been used to separate SOC into distinct components with varying turnover times (Townsend et al., 1995; Trumbore et al., 1989). However, recent ^{14}C analyses of non-fractionated, bulk SOC from Louisiana and Saskatchewan displayed homogenized downcore ^{14}C age spectra (Plante et al., 2013; Vetter et al., 2017). Similar analyses from soils in Liberia and Hawaii revealed the same downcore ^{14}C trends (Rosenheim, 2019, *personal communication*). These results suggested SOC at each site was controlled by a single, dominant turnover time.

Carbon stabilization influences the mixing and degradation of SOC and therefore, the timescale of carbon storage. Stabilization of SOC in upland environments is thought to be the result of selective preservation, mineral-binding, microbial activity, and/or environmental conditions (Hemingway et al., 2019; Lehmann and Kleber, 2015; Schmidt et al., 2011; Steinmuller and Chambers, 2019). Wetland research has begun to examine whether the mechanisms responsible for SOC stabilization in upland environments are the same for coastal habitats. These studies invoke similar stability mechanisms including changes in OC quality, microbial control, and environmental conditions (Breithaupt et al., 2020; Steinmuller and Chambers, 2019). Yet, this research has led to conflicting conclusions due to the limited focus specifically on mechanisms of SOC stabilization in wetlands. A study from a Louisiana wetland found soil organic matter remained degradable to a depth of 150 cm, suggesting any stabilized carbon was the result of *in situ* microbial or environmental processes, rather than an inherent property of the soil (Steinmuller and Chambers, 2019). Yet, work from a nearby site revealed decreased thermochemical stability

of SOC with increasing salinities, indicating a change in environmental conditions may destabilize wetland carbon stores (Williams and Rosenheim, 2015).

In this study, I employ a multi-proxy approach to examine SOC cycling and stabilization in mangrove soils. A variety of radiometric geochronometers (^{210}Pb , ^{137}Cs , and ^{14}C) paired with stable carbon isotopes, elemental analysis, downcore lignin profiles, and activation energy distributions help to provide insight into mangrove SOC dynamics.

Lead-210 is a naturally-occurring fallout radionuclide from the ^{238}U decay series with a half-life of 22.3 years (Appleby and Oldfield, 1978). Its short half-life makes it a useful chronometer over the last century. Dates determined from ^{210}Pb models are often supported using additional radionuclides such as ^{137}Cs , an anthropogenic radionuclide produced from thermonuclear weapons testing (Abril, 2004; He and Walling, 1997). Correlation of ^{210}Pb soil ages with peak Northern Hemisphere ^{137}Cs fallout in 1963 allows for independent age verification. However, ^{137}Cs has been shown to migrate post-deposition and therefore its validity as a geochronometer must be validated (Abril, 2004; Drexler et al., 2018; Morris et al., 2000). In addition, due to its continual decay and the lack of new atmospheric fallout, ^{137}Cs activities in the Northern Hemisphere are barely above detection limits, making measurements even more challenging (Drexler et al., 2018).

The establishment of an independent ^{210}Pb chronology allows for the interpretation of ^{14}C solely as a tracer of the ^{14}C bomb peak and as a means to examine SOC cycling. Two forms of ^{14}C dating of OC were used in this study – conventional bulk analysis and Ramped PyrOx. Whereas bulk analysis gives a single age for a sediment interval, Ramped PyrOx allows for the determination of a spectrum of ages within a single sample (Rosenheim et al., 2008). Ramped PyrOx is based on the thermochemical stability of organic matter which allows for the distinction

of young, labile components from older, refractory components within the SOC pool. This makes it a valuable tool to investigate SOC cycling because it provides an analytical method to separate distinct pools of carbon within a soil (Plante et al., 2013; Vetter et al., 2017).

Activation energy distributions provide another way to assess the stability of organic carbon both within and between sites. Hemingway et al., (2017) developed a regularized inverse method to convert Ramped PyrOx ^{14}C values into activation energy distributions. The CO_2 decay profiles generated from Ramped PyrOx are potentially useful for assessing the thermochemical stability of a sample; however, they can be impacted by experimental conditions and oxidation pathways (Hemingway et al., 2017). Activation energy, a proxy for bond strength, is independent of these confounding conditions, making it an accurate and useful tool for determining SOC stability.

Lignin phenol ratios also lend insight into the stability of organic matter. Lignins are polymers sourced from the cell walls of vascular plants (Hedges and Mann, 1979). Oxidation of lignin produces a variety of phenols that preserve many of the same characteristics of the original polymer which has led to their widespread use as a tracer of terrestrial organic matter input (Hedges and Mann, 1979). In addition, the ratios of lignin phenols can be used to assess degradation. The ratio of vanillic acid to vanillin $(\text{Ad}/\text{Al})_v$ represents the degree of degradation *between* samples or sites (Ertel and Hedges, 1984). Lignin:OC profiles are used to determine changes in degradation *within* a site and relative changes in mineralization downcore.

This study will identify and quantify the mechanisms responsible for carbon movement and stabilization in mangrove soils through a multi-proxy approach using peat cores from Ten Thousand Islands, Florida. A better understanding of these mechanisms will help to constrain

current carbon stock estimates and will aid in our understanding of the impact of SLR on mangrove soil stores and whether these systems will remain a sink of carbon in the future.

1.1 Research Questions

To better understand the processes driving in situ SOC movement and stabilization in mangrove wetlands, several questions must be addressed:

1. Does *in situ* carbon movement impact the size of mangrove carbon stock in the top 25-cm of soil?
2. What is the timescale of carbon storage in mangrove soils?
3. What are the mechanisms controlling mangrove carbon stability?

Chapter 2. Methods

2.1 Study Site and Core Collection

The soil cores used in this study were collected from the Ten Thousand Islands region of southwest Florida (Figure 6). The islands within the region are antecedent highs built by oyster and vermetid gastropod reefs and later colonized by mangroves (Shier, 1969). The underlying substrate at Ten Thousand Islands can be divided into three major units. Miocene limestone underlies the entire region, followed by marsh sediments formed during the Wisconsin low sea level stand, and finally sediments deposited from a marine transgression throughout the post-Wisconsin sea level rise (Shier, 1969).

Two cores were collected from an overwash mangrove island near the mouth of the Upper Faka Union Canal, referred to here as the open mangrove site (Figure 6). This site is exposed to nearly constant flushing as a result of water flow from the canal and daily tidal fluctuations from the nearby Gulf of Mexico (5 km). Two additional cores were collected from the Cat's Claw Basin, referred to here as the confined mangrove site (Figure 6). Although this site is at a similar distance (5 km) to the Gulf of Mexico, it experiences reduced tidal flow due to the presence of a berm along the western edge of the forest and raised road to the north. Aerial imagery from the site indicates Between 1952 and 1963 the road was constructed, and the natural berm was enhanced, further restricting water flow. Both sites are dominated by red (*Rhizophora mangle*) and black (*Avicennia germinans*) mangroves with sporadic white (*Laguncularia racemosa*) mangroves. At each site a short push core (~25 cm) and a longer Russian core (50-100 cm) was taken and stored in a cooler until returned to the laboratory.

2.2 Soil Composition

Loss on Ignition

The loss on ignition (LOI) technique was used to determine the dry bulk density (DBD), organic matter, and carbonate content for each soil interval. Cores were sliced at 1 cm intervals and a known volume/aliquot (4.15 cm³) of sediment was removed. Dry weight was determined by drying aliquots in pre-baked ceramic crucibles for 24 hours at 105°C in a muffle furnace, while DBD was calculated by dividing dry weight by the aliquot volume. The aliquots were then heated for 3 hours at 550°C and weighed. The percentage of organic matter in each interval was determined by dividing the 550 weight by the dry weight and multiplying by 100. The inorganic content was determined by drying the remaining material at 950°C for 2 hours. Carbonate content was calculated by subtracting 950°C weight from 550°C weight.

Elemental Analysis

Soil from radiocarbon dated intervals was analyzed for percent total organic carbon (%TOC), %N, and %C using an Elementar vario MICRO elemental analyzer at the University of South Florida. Prior to analysis, samples were sieved (<63 µm) and acid treated with 1N HCl to remove potentially time transgressive material (e.g. root hairs) and carbonates, which have the potential to bias sample ages. Sample weight



Figure 2 Image of an unsieved sample from the confined mangrove site. Samples were placed under a microscope and root hairs were divided by size class. Scale bar represents 1 mm.

constraints were determined based on detection limits for the instrument (100-300 $\mu\text{g N}$, 400-1000 $\mu\text{g C}$) before samples were weighed and loaded into tin capsules. Blocks of 5 samples were alternatively run with sets of standards, in order to constrain blank values, that included an empty tin capsule, acetanilide, and sorghum flour.

Additionally, root hairs from unsieved, acid treated samples were picked under a microscope and divided into large (>1 mm) and small (≤ 1 mm) groups (Figure 2), to determine the influence of root hairs on soil chemical composition. Root hairs were then packed into tin capsules and sent to the National Ocean Sciences Accelerator Mass Spectrometry (NOSAMS) facility to be analyzed for %TOC, %N, %C, $\delta^{13}\text{C}$, and ^{14}C . Samples were injected into the elemental analyzer and the eluded CO_2 was then channeled into the AMS for ^{14}C dating. C:N ratios were calculated for all samples to constrain the source of organic matter.

Lignin Content

Lignin phenols were extracted and analyzed using the cupric oxide method from Hedges and Ertel (1982), later modified by (Louchouart et al., 2010), and previously published in (Breithaupt et al., 2020). Of importance to this study are the lignin oxidation products vanillin and vanillic acid, and the total lignin content. The acid/aldehyde ratio of vanillyl phenols (Ad/Al)_v is used to assess the extent of degradation *between* sites and samples, with a higher ratio indicating a greater degree of degradation (Ertel and Hedges, 1984). The degree of degradation *within* the soil column can be determined using downcore lignin:OC profiles and is based on the assumption that lignin is relatively stable in comparison to OC (Breithaupt et al., 2020). Lignin:OC ratios do not provide insight into the magnitude of degradation and therefore cannot be used to compare sites. However,

these ratios can be used to tell relative differences, making them useful for understanding intra-site variation in degradation and mineralization.

2.3 Chronometers

Lead-210 and Cesium-137

The two shorter push cores from the open and confined mangrove sites were ^{210}Pb -dated at the US Geological Survey in St. Petersburg, Florida, using methods previously described by Smoak et al., (2013). Sediment ages and mass accumulation rates were determined using the Constant Rate of Supply (CRS) model (Appleby and Oldfield, 1978). This model was chosen because of the assumption of a variable sedimentation rate, with a constant supply of ^{210}Pb , over the course of the record. Analysis of downcore ^{210}Pb profiles also provides a way to assess the potential impact of bioturbation. Cesium-137 peaks were not used to confirm ^{210}Pb dates because of their displacement from the period maximum ^{137}Cs fallout (~1963) which indicated the cesium had migrated post-deposition. However, storm deposits from hurricanes Wilma (2005), Andrew (1992), and Donna (1960) aligned with ^{210}Pb dates, providing an independent source of age verification.

Radiocarbon (^{14}C)

Radiocarbon Sample Preparation

The two longer Russian cores from the open and confined mangrove sites were ^{14}C dated to extend the length of the ^{210}Pb chronology and investigate SOM cycling mechanisms. Two preparation methods were employed in order determine the ^{14}C content of samples – bulk combustion and Ramped PyrOx. Both preparation methods require either fresh or freeze-dried

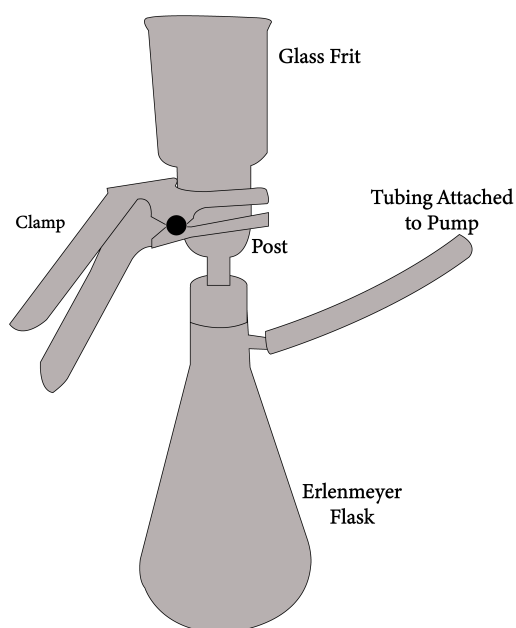


Figure 3 Schematic of filtration apparatus. Quartz fiber filters are placed between the post and frit and secured in place with the clamp.

samples to be sieved and acid treated to remove roots, large particles, and carbonates. If transported through the sediment column, large particles such as roots, can provide skewed ages if dated. Carbonates show up as a distinct high-temperature peak on a Ramped Pyrox thermograph and also have the potential to bias radiocarbon ages. Samples were mixed with 2000 mL of water and passed through 500 and 63 μm sieves, creating a sediment slurry of particles $<63 \mu\text{m}$. The 2000 mL of sieved sediment slurry was then filtered through four pre-combusted (900°C , 4 hours) and weighed

quartz fiber filters – with approximately 500 mL of slurry passing through each filter. Figure 3 displays the filtering apparatus which includes a post that supports the filter, a glass frit which holds the sediment slurry, and a clamp. Once filtration was complete, filters were dried in a muffle furnace at 50°C for 24 hours. Filters were returned to the same filtration set-up (Figure 3), submerged in 1N HCl for 30 minutes, and subsequently rinsed with deionized (DI) water until a pH of 6 was reached. Filters were then dried at 50°C for another 24 hours.

A number of samples were prepared separately in order to investigate possible mechanisms related to carbon transport in the soil column. Twelve intervals were acid treated, but not sieved, prior to analysis in order to examine the influence of root hairs on carbon transport. In addition, 8 samples were acid-base-acid (ABA) treated to understand the influence of humic acids on carbon

transport. Sediment-laden filters were submerged in 1N HCl for 30 minutes and then rinsed with 1N NaOH. NaOH was run through filters until the supernatant was clear. Filters were then submerged in 1N HCl for another 30 minutes before being rinsed with DI water until a pH of 6 was reached and dried at 50°C for another 24 hours in a muffle furnace.

Ramped PyrOx

Ramped PyrOx (discussed in detail in Rosenheim et al., 2008) is a ^{14}C preparation method that separates SOM based on thermochemical stability, allowing for the determination of a spectrum of ^{14}C ages within a single sample. Sieved and acid treated samples were weighed in order to yield a total of ~100 micromoles of CO_2 which was determined stoichiometrically from %TOC established from elemental analysis. The CO_2 generated from Ramped PyrOx was divided into approximately five aliquots, or sub-samples, of 20 μmol each. Each aliquot was cleaned of non-condensable gases and water using liquid nitrogen and an isopropyl slush cooled to phase transition with liquid nitrogen (-77°C), before being sealed into a pre-combusted Pyrex tube (550°C, 4 hours) loaded with 1 cm of silver wire and 150 mg of CuO. Once samples were sealed, they were redundantly combusted at 550°C for 4 hours in a muffle furnace before being sent to NOSAMS for ^{14}C dating and $\delta^{13}\text{C}$ measurements.

Bulk Combustion

When compared to Ramped PyrOx, bulk combustion of soil samples provides a relatively inexpensive and easy way to obtain ^{14}C dates. In systems with multiple sources of OC, Ramped PyrOx provides greater insight into the nuances of sample composition. However, initial analyses ($\delta^{13}\text{C}$ and ^{14}C) indicated samples from the open and confined mangrove sites were dominated by

a single source of OC. In this case, bulk combustion provided similar insight into SOC dynamics as Ramped PyrOx (Figure 1A).

Samples were weighed in order to yield between 25-50 μmol of CO_2 which was determined stoichiometrically from %TOC established from elemental analysis. Weighed samples were transferred into pre-combusted quartz tubes (900°C , 4 hours), loaded with 1 cm of silver wire and 150 mg of CuO. Tubes were connected to a vacuum line, evacuated of atmospheric gases, and flame sealed to ensure samples remained under vacuum during combustion. Sealed tubes were combusted in a muffle furnace at 900°C for 4 hours, converting organic matter to CO_2 . Tubes were reattached to the vacuum line where they were cracked in order to purify the sample of water vapor using liquid nitrogen and isopropyl slush cooled to phase transition with liquid nitrogen (-77°C). Once purified, the gas volume was manometrically quantified, and the CO_2 was re-sealed into a pre-combusted Pyrex tube (550°C , 4 hours). All samples were sent to NOSAMS for ^{14}C dating and $\delta^{13}\text{C}$ measurements.

Blank Correction

Radiocarbon values determined from both Ramped PyrOx and bulk sample preparation were blank-corrected following analysis at NOSAMS. Blank correction follows the methods of Fernandez et al., (2014), where the measured fraction modern (Fm) of a sample can be written as a mixture of three components: the Fm of the unknown sample material, the radiocarbon “dead” blank, and the “modern” radiocarbon blank. Dead blank was assessed using an oxalic acid standard, whereas modern blank was assessed using a graphite standard. Table 1 lists the modern and dead blank values for Ramped PyrOx and bulk combustion.

Table 1 Modern and dead blank values for Ramped PyrOx and bulk combustion.

Type of Blank	Method	Value \pm Analytical Error (μg)
Dead Blank	Ramped PyrOx	1.1586 \pm 0.9067
Modern Blank	Ramped PyrOx	2.5236 \pm 1.6502
Dead Blank	Bulk Combustion	2.2738 \pm 2.0738
Modern Blank	Bulk Combustion	4.5132 \pm 1.8302

2.4 Data Analysis

Activation Energy Distributions – rampedpyrox Python Package

Hemingway et al. (2017) developed a regularized inverse method to determine SOC activation energy distributions, a proxy for bond strength. The open-source Python package “rampedpyrox” was used to convert Ramped PyrOx data outputs into activation energy distributions which were then used to assess the stability of SOC (Hemingway, 2016). Specifically, for each sample, the CO₂ decay profile and isotopic data from Ramped PyrOx was organized into two data files to generate activation energy distributions. The first data file includes three columns (date_time, temperature, CO₂) and represents the evolution of CO₂ for a sample. The second data file includes seven columns (date_time, fraction, ug_fraction, $\delta^{13}\text{C}$, $\delta^{13}\text{C}$ _error, Fm, Fm_error) and represents the isotopic composition of a sample. Fraction refers to each aliquot, or sub-sample, of CO₂, with generally 5 fractions per sample. The amount of CO₂ per fraction is converted into micrograms (ug_fraction) and the corresponding stable carbon isotopic data ($\delta^{13}\text{C}$), radiocarbon data (Fm), and associated errors are recorded ($\delta^{13}\text{C}$ _error, Fm_error).

The utility of Ramped PyrOx, or any serial decomposition (oxidation or pyrolysis) method, comes from separating a complex mixture of organic matter into discrete components with similar physical and/or chemical properties and measuring the isotopic composition of each component ($\delta^{13}\text{C}$, ^{14}C). Using this information to inversely model activation energy distributions allows us to obtain a quantifiable measure of the stability of organic matter.

Turnover Time

Input (I) and decomposition (k) values for the open and confined mangrove sites were determined from a model of carbon accumulation at both sites. Cumulative carbon plots were made by plotting cumulative carbon inventory (kg C m^{-2}) versus years before sampling. Equation 1 represents the soil layer C inventory (kg C m^{-2}) in year t . Equation 1 was fit to the cumulative carbon curves using a nonlinear regression function in MatLab which adjusts input ($\text{kg C m}^{-2} \text{ y}^{-1}$) and decomposition (y^{-1}) values until the best fit is achieved (Figure 4). A Monte Carlo simulation with 10,000 iterations was then used to generate a probability distribution of I and k values based on equation 1 and the uncertainties for each associated variable (Table 2). Figure 5 displays the probability distributions for the I and k parameters for the open and confined mangrove sites and the associated error.

$$C(t) = \left(\frac{I}{k}\right) \times (1 - e^{-kt}) \quad (1)$$

Table 2 Input variables, input error, output variables, and output error for the Monte Carlo simulation. Input error on cumulative carbon content was fixed because error in carbon content was ultimately linked back to error in age (e.g. years before present). Input error for years before present is presented as a range of values because error varied based on depth with error increasing with increased depth/age.

Open Mangrove			
Input Variables	Input Error	Output Variables	Output Error
Cumulative Carbon Content (kg C m^{-2})	0.1% of carbon content	Input, I ($\text{kg C m}^{-2} \text{ y}^{-1}$)	0.0027
Years Before Present	0.5 – 5.51 years	Decomposition, k (y^{-1})	6.04×10^{-4}
Confined Mangrove			
Input Variables	Input Error	Output Variables	Output Error
Cumulative Carbon Content (kg C m^{-2})	0.1% of carbon content	Input, I ($\text{kg C m}^{-2} \text{ y}^{-1}$)	0.0036
Years Before Present	0.47-7.89 years	Decomposition, k (y^{-1})	9.07×10^{-4}

Turnover time (τ) was then calculated with equation 2, using the k value determined from the probability distribution and the associated error.

$$\tau = \frac{1}{k} \quad (2)$$

Equation 2 is valid only in autonomous, single pool, linear, steady-state systems. The only assumption not met by the open and confined sites is autonomy, which would indicate the environment has no effect on the rate at which carbon is cycled in a system (Sierra et al., 2017). However, this estimation of turnover is congruent with past efforts in other upland systems and provides a starting point from which differences can potentially be attributed to autonomy of the system.

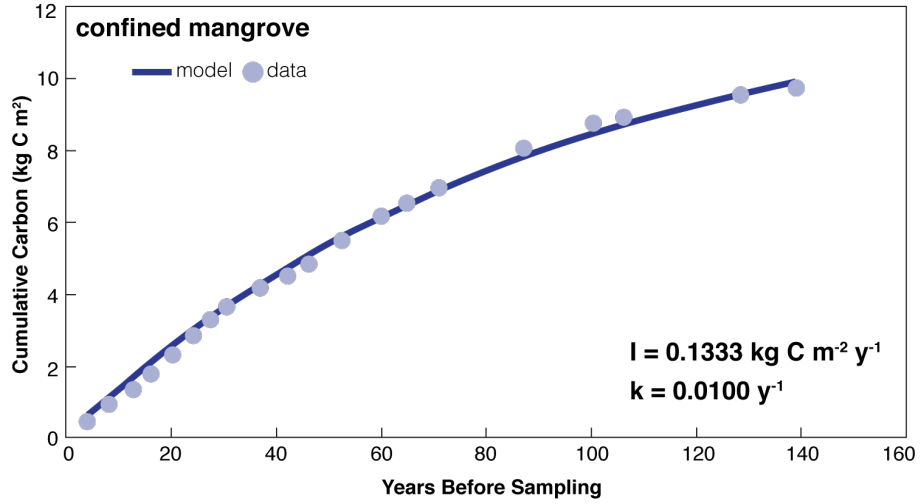
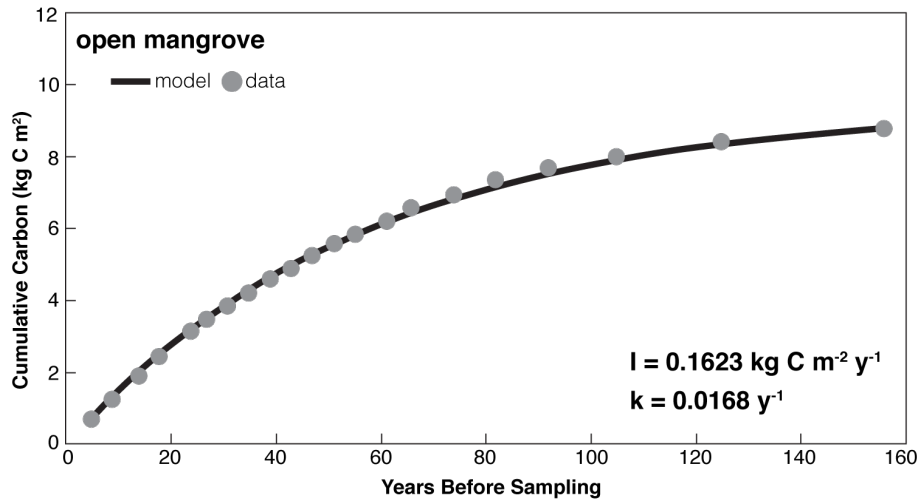


Figure 4 Cumulative carbon plots for open and confined mangrove sites. Dots represent cumulative organic carbon burial over time. Equation 1 was fit to the cumulative carbon curves using a nonlinear regression function to get modeled values (lines).

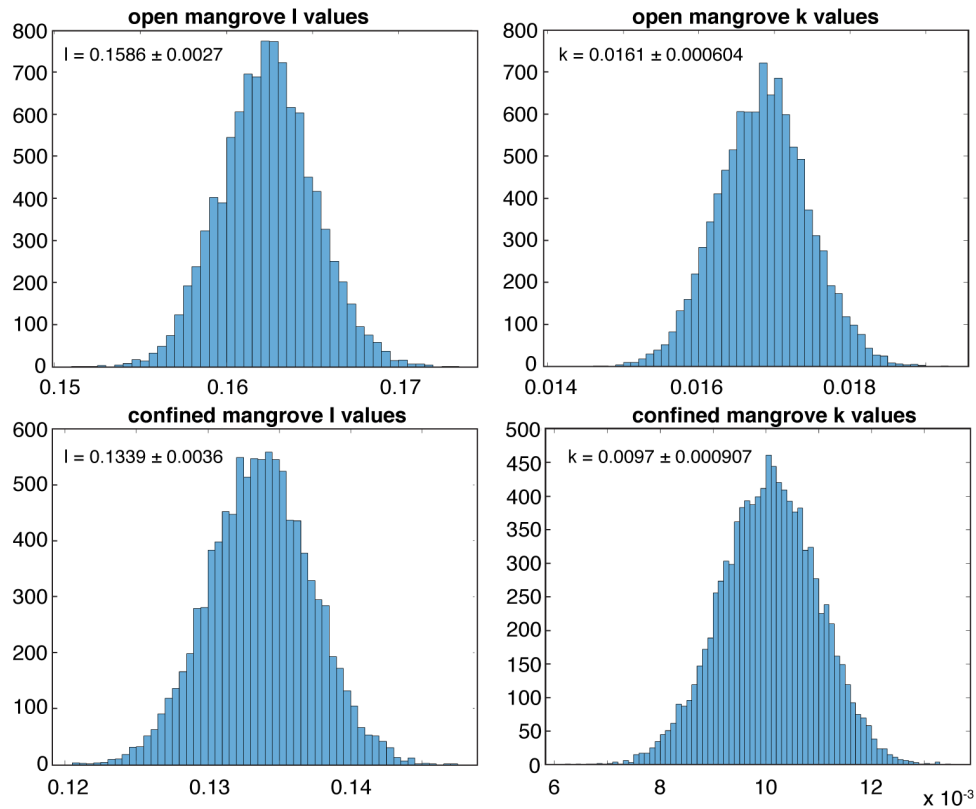


Figure 5 Probability distributions for input (I) and decomposition (k) values for the open and confined mangrove sites. Values were generated using a Monte Carlo simulation with 10,000 iterations. Error on values is standard deviation.

Chapter 3. Mangrove Carbon Storage Efficiency Facilitated by Young Carbon Transport

The following chapter is written in the form of a manuscript to be submitted for publication.

Carey Schafer, Brad E. Rosenheim, Joseph M. Smoak, Ryan P. Moyer, Joshua L. Breithaupt, Christopher G. Smith, Derrick R. Vaughn, Thomas S. Bianchi.

Abstract

Globally, mangrove forests have the highest carbon storage capacity among vegetated terrestrial habitats, despite occupying a smaller spatial extent (Alongi, 2014; Donato et al., 2011). Many studies have focused on quantifying soil carbon stock in an effort to underscore the effectiveness of the mangrove carbon sink (Alongi, 2014; Breithaupt et al., 2012). However, quantification of stock alone ignores the mechanisms governing *in situ* soil organic carbon (SOC) cycling and stability which mediate the timescale of carbon storage and therefore inform our understanding of mangrove carbon storage efficacy. Here we use radiocarbon values paired with a ^{210}Pb chronology to investigate SOC cycling in mangroves in Ten Thousand Islands, Florida. We present a novel SOC transport mechanism, whereby young carbon is transported in pore waters to a depth of at least 32 cm. We argue this young carbon is sourced from root exudates and stabilized through microbial processing before being transported to depth in pore waters. A comparison of two sites experiencing variable tidal regimes (inundation vs. tidal flushing), revealed inundation serves to enhance stability, but does not appear to be the driving factor behind mangrove SOC stability.

Mangrove forests store significantly more carbon per unit area than any other vegetated terrestrial ecosystem (Mcleod et al., 2011). Because of this high capacity for carbon storage, mangroves are recognized as important natural carbon sinks despite occupying a relatively limited spatial extent along tropical and sub-tropical coastlines (Mcleod et al., 2011). Many studies have quantified soil carbon stock as a way to highlight the effectiveness of the mangrove carbon sink (Alongi, 2014; Breithaupt et al., 2012; Donato et al., 2011). However, quantifying stock alone fails to fully capture why mangrove soils are so efficient at storing carbon because this simple quantification ignores *in situ* soil organic carbon (SOC) dynamics that mediate carbon storage. The majority of mangrove carbon is stored in soils that are waterlogged and rich in organics (Donato et al., 2011). These conditions promote the long-term accumulation of soil organic carbon (SOC) because, through oxygen-depletion, they prevent the microbial breakdown of organic matter (Alongi, 2014; Kristensen et al., 2008).

Anaerobic conditions in mangrove soils are ultimately modulated by rates of carbon input and export/decomposition. What remains in the soil has often been characterized as multiple pools of different ages and distinct turnover times (Jenkinson and Rayner, 1977; Trumbore, 2000). Variation in turnover time is the result of differences in SOC stability. Upland terrestrial soil research has used both numerical and conceptual modeling to understand the role of organic matter composition, microbial activity, and mineral interactions in stabilizing SOC (Hemingway et al., 2019; Schmidt et al., 2011). However, it is unknown whether the same biogeochemical factors influencing SOC stability in upland terrestrial ecosystems influence SOC stability in mangrove soils and whether these multi-pool models accurately reflect the natural dynamics of mangrove soils and their timescales of carbon storage.

In this study, we aim to identify and quantify the mechanisms responsible for SOC transport and stabilization in mangrove soils. We found mangrove soils are transporting young carbon, sourced from root exudates, in pore waters to a depth of at least 32 cm. Microbially processing of root exudates acts to initially stabilize the young carbon, while inundation serves to enhance stability which is reflected in the variation in turnover time between sites experiencing differing tidal regimes. Knowledge of these processes is necessary to understand why mangrove soils are so efficient at trapping carbon and whether these mechanisms may be impacted by future climate change (Bardgett, 2011; Zhai et al., 2013).

To assess carbon transport and stability in mangrove wetlands, we analyzed 4 peat cores from two sites in Ten Thousand Islands, Florida, USA (see Chapter 2). These sites, referred to as the open mangrove and confined mangrove sites, were chosen based on differences in tidal influence (Figure 6). The open mangrove site experiences daily tidal fluctuations that introduce



Figure 6 Map of study sites in Ten Thousand Islands, Florida, USA. Panels on the right display each location's varying tidal influence. The confined mangrove site is protected from tides by a sediment berm, whereas the open mangrove site experiences daily tidal flushing.

oxygen-rich waters into the system. The confined mangrove site is protected from tides by a sediment berm, leaving soils inundated, but infrequently flushed with water. Both the open and confined

mangrove sites are dominated by mixture of red (*Rhizophora mangle*) and black (*Avicennia*

germinans) mangroves. From these cores, we generated “bomb” radiocarbon (^{14}C) records for mud sized particles ($< 63 \mu\text{m}$) using both Ramped PyrOx and bulk combustion (see Chapter 2; Figure 1A). We coupled the resulting ^{14}C records with an independent ^{210}Pb chronology at each site to constrain soil ages and used ^{137}Cs profiles to investigate mechanisms of soil transport because of the mobile nature of ^{137}Cs in wetland soils (Drexler et al., 2018).

We interpreted radionuclide records in conjunction with other isotopic and chemical proxies of carbon source ($\delta^{13}\text{C}$, C:N ratios, $\%\text{CO}_3$) and organic matter stability ($(\text{Ad}/\text{Al})_v$ ratios) (see Chapter 2). The ratio of two lignin phenols, $(\text{Ad}/\text{Al})_v$, was used to assess stability between samples or sites (Ertel and Hedges, 1984). To complement the geochemical proxies of source and stability, we used activation energy, a proxy for bond strength, to assess the stability of organic carbon at each site. We employed a regularized inverse method to convert decomposition data from Ramped PyrOx into activation energy distributions (Hemingway, 2016; Hemingway et al., 2017). This method allowed us to apply useful data from Ramped PyrOx (^{14}C , $\delta^{13}\text{C}$) independently of confounding variables (e.g. experimental conditions, oxidation pathways) to accurately assess the relationship between soil age and stability.

In order to understand SOC transport, we analyzed ^{210}Pb chronologies in conjunction with profiles of ^{14}C from sieved mud samples ($<63 \mu\text{m}$) from the open and confined mangrove sites. We detected the penetration of bomb ^{14}C ($F_m > 1$) in soils ^{210}Pb -dated back to 1892, indicating the post-depositional migration of SOC (Figure 7). In upland terrestrial ecosystems, soils have been modeled as a mixture of carbon pools, with turnover times ranging from years to millennia (Jenkinson and Rayner, 1977; Trumbore, 2000). Based on an upland multi-pool model of SOC cycling, the young ^{14}C signature may represent a single distinct carbon pool within the bulk soil,

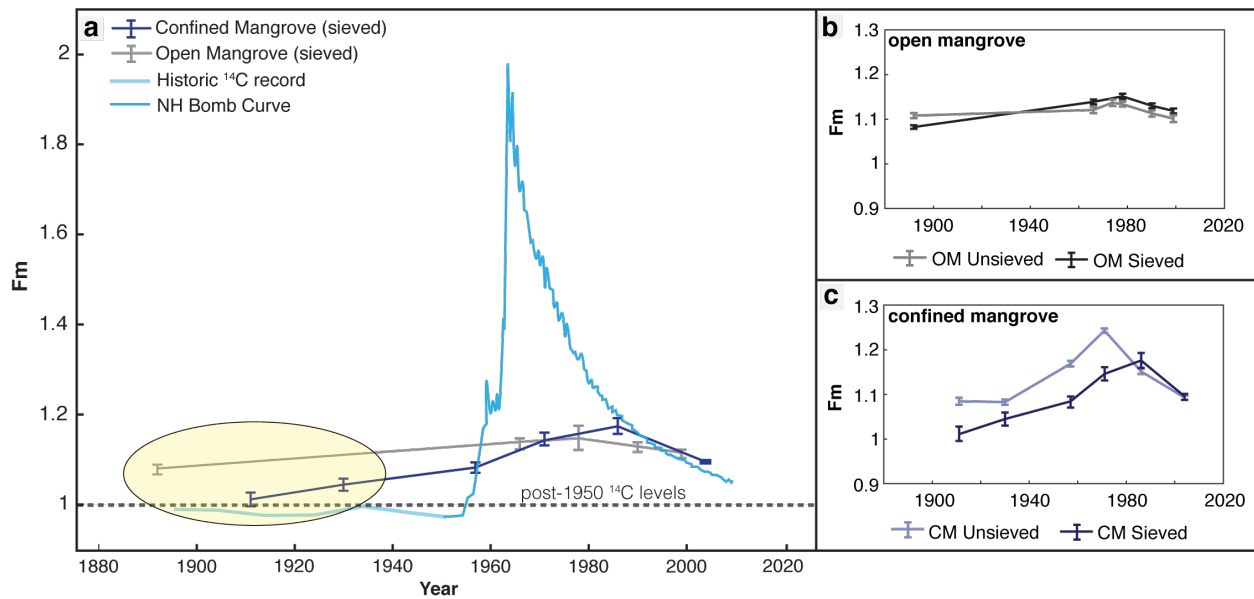


Figure 7 Radiocarbon (^{14}C) results from the open and confined mangrove sites in Ten Thousand Islands, Florida. A) Comparison of atmospheric ^{14}C bomb spike to ^{14}C values from sieved samples at both sites. Yellow circle highlights intervals where post-depositional movement of carbon is apparent due to $F_m > 1$. B, C) Comparison on ^{14}C values for unsieved and sieved samples from the open mangrove site and the confined mangrove site. The similarity in curve shape and ^{14}C values indicates the young ^{14}C signature is representative of the bulk soil organic carbon (SOC). For all figures, error bars incorporate analytical error and blank correction.

differentiated by both size fraction ($<63\ \mu\text{m}$) and age. To make claims about carbon cycling on an ecosystem-wide scale, we needed to determine whether the young ^{14}C signature was representative of the bulk soil, or a small component of a multi-pool system. To test this, we generated ^{14}C records of unsieved SOC at both sites. The ^{14}C values and trends from the sieved samples aligned with unsieved samples (Figure 7), which suggested the young ^{14}C signature of sieved material represents the bulk soil pool, rather than a small SOC fraction of a multi-pool system.

The movement of young carbon to depth highlights a previously unrecognized mangrove SOC transport mechanism and underscores why mangrove soils are such effective sinks of carbon. Our data suggest young carbon is transported to a depth of at least 32 cm. This movement allows mangroves to continually add to mangrove SOC stocks through the downward movement of carbon. Using an annual OC burial rate of $123\ \text{g m}^{-2}\ \text{yr}^{-1}$ (Breithaupt et al., 2014) and a two-end

member ^{14}C mixing model (Tables 1A, 2A), we estimate over the last 120 years, the downward transport of young carbon alone has contributed to the burial of 184 Tg of carbon in mangrove soils, globally (13,776,000 ha) (Giri et al., 2011).

Identifying the mechanism(s) responsible for the downward transport of young carbon is vital for assessing the on-going efficacy of the mangrove carbon sink and whether the transport and storage of young carbon will be impacted by future climate change. Determining the mode of transport (particle-associated or dissolved), can lend insight into the source of young carbon and the impact climate change may have on this transport mechanism. To differentiate between these two types of SOC transport, we analyzed profiles of ^{210}Pb , ^{137}Cs , and ^{14}C . The similarities between downcore ^{14}C profiles and ^{137}Cs profiles suggest that porous mangrove peats allow for young carbon transport in the dissolved phased via pore water advection. The decline of excess ^{210}Pb activity at an exponential rate indicates ^{210}Pb did not migrate post-deposition (Figure 8). However, post-depositional transport impacted both ^{14}C and ^{137}Cs profiles as evidenced by the bomb ^{14}C signature to a depth of at least 32 cm and the displacement of the ^{137}Cs peak at both sites (Figure

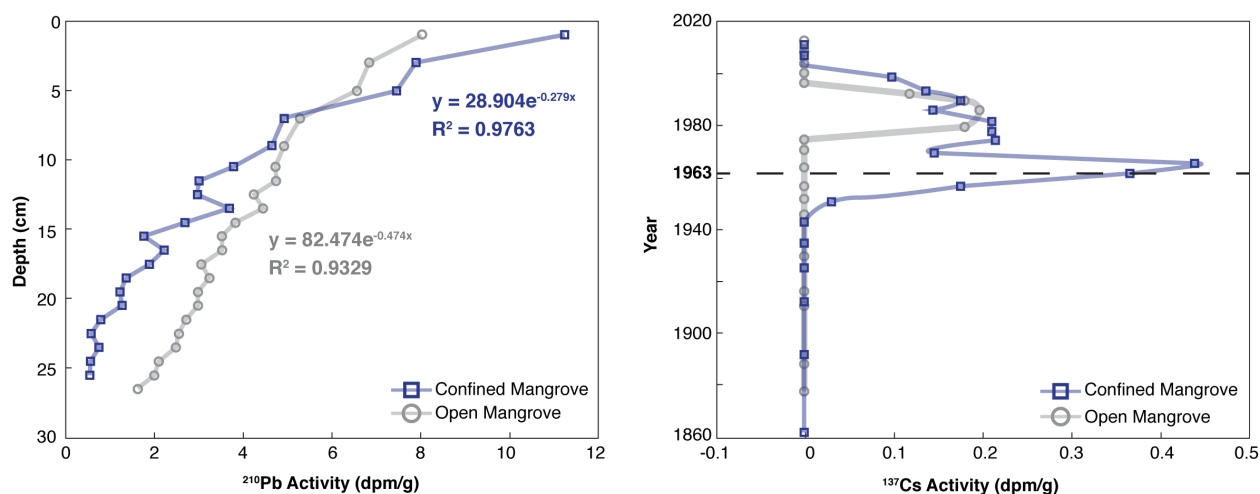


Figure 8 Downcore profiles of ^{210}Pb and ^{137}Cs . The exponential decline in ^{210}Pb activity indicates ^{210}Pb was not transported post-deposition. Peak ^{137}Cs fallout should occur at 1963. At both sites, the peak is displaced, indicating ^{137}Cs migrated post-deposition.

8). The differences in post-depositional transport (or lack thereof) represent independent sedimentary and pore water processes acting on the soil column. ^{210}Pb has a strong particle affinity and therefore its distribution is largely reflective of the sedimentary processes occurring within the soil column (Carpenter, 1997). Its strong particle affinity, paired with its exponential downcore profile (Figure 8), indicate ^{210}Pb was not transported to depth in association with particulate carbon; therefore, the bomb ^{14}C must have been transported to depth through a different mechanism. ^{137}Cs has a lower particle affinity than ^{210}Pb , allowing it to enter into solution through pore water advection (Carpenter, 1997; Morris et al., 2000). Similarly, when soils are exposed to water flow, dissolved organic carbon (DOC) can be released into pore waters and re-absorb onto particle surfaces deeper in the soil column (Gross and Harrison, 2019; Sanderman et al., 2008).

Despite ^{210}Pb and ^{137}Cs profiles indicating young SOC is transported in pore waters, we considered commonly cited SOC transport mechanisms in wetland soils, including those that are particle-associated. We investigated the contribution of bioturbation, humic acids, root hairs, and carbonate dissolution to the young ^{14}C signature at the open and confined mangrove sites. Downcore ^{210}Pb trends and ^{14}C dates indicate none of these mechanisms explain our data set (Figures 2A, 3A; Appendix A) and provide another line of evidence for dissolved carbon transport, rather than particle-associated downward advection. Previous studies have highlighted the role of tidal flushing in driving the export of carbon from mangrove soils (Maher et al., 2013). Our two study locations, the open and confined mangrove sites, experience differences in tidal influence, allowing us to assess the influence of tides on *in situ* carbon transport. Both sites display similar downcore ^{14}C and $\delta^{13}\text{C}$ trends (Figures 7, 4A), despite variations in tidal influence, indicating tidal flushing is likely not driving the downward transport of young carbon.

Our data suggest the high porosity of mangrove peats (~40-70% in the Gulf of Mexico) creates natural conduits that allow for the downward percolation of porewaters transporting young carbon to a depth of at least 32 cm. The flattened shape of the bomb curve indicates some of this young carbon is lost via pore water export; however, that which remains in the system is stabilized in the particulate form. Previous research has demonstrated the link between young ^{14}C signatures and thermochemical stability, with more labile SOC components exhibiting younger ages (Rosenheim et al., 2008; Rosenheim and Galy, 2012). This would suggest the young carbon present at both of our sites is relatively degradable with a short turnover time. To better constrain the timescale of carbon storage, we modeled SOC turnover and determined a turnover time of 62 ± 0.09 years for the open mangrove site and 103 ± 0.91 years for the confined mangrove site for the top 25 cm of soil at both sites (Sierra et al., 2017) (see Chapter 2; Appendix A). Soil turnover at each site indicates SOC is relatively stable, despite its young ^{14}C signature and its location within a zone of active microbial reworking.

In upland terrestrial research, SOC stability has been attributed to organic matter composition and/or ecosystem properties (e.g. inundation, mineral binding, microbial interactions) (Schmidt et al., 2011). The presence of young, stabilized carbon in an active soil layer at both of our sites raises the question as to whether the young carbon is inherently stable or if its stability is environmentally mediated. Our two sites were chosen due to differences in tidal influence, yet both show the transport of young carbon to depth. This would suggest that ecosystem properties are not fundamentally driving SOC stabilization from the dissolved to particulate phase. Our results preclude humic acids and root hairs as possible sources of young carbon to the environment (Figures 2A, 3A). In addition, we know young carbon is transported via pore water advection, ruling out leaf litter sourced from mangroves. We hypothesize it is the production of root exudates,

transported downward in pore waters, and subsequent microbial processing which provides the ultimate source of stabilized particulate carbon at our sites.

Whereas root exudates are generally considered an active pool of carbon with a rapid turnover, previous research has suggested a substantial proportion of bulk SOC is derived from root exudates (Derrien et al., 2004; Torn et al., 2009). We argue this microbially processed root-derived carbon is transported downward via pore water advection and stabilized in the particulate form through adsorption. Chemical analysis of root exudates indicates they can be rapidly converted to microbial byproducts, while rhizospheric sugars display a time-increasing signature of bulk SOC (Derrien et al., 2004), suggesting microbial transformation acts to stabilize root exudate-derived carbon long term. Additionally, research on the composition of the soil DOC pool has indicated the microbial release of labile plant-derived compounds is the dominant process maintaining the soil DOC pool (Sanderman et al., 2008; Van Hees et al., 2005). The prevalence of root-derived carbon in the DOC pool and evidence of microbially mediated adsorption give weight to this interpretation (Lehmann and Kleber, 2015). This explanation aligns with the Microbial Efficiency-Matrix Stabilization (MEMS) framework which argues, despite relatively low input rates, labile plant constituents are preferentially processed by microbes because they are utilized more efficiently than other inputs (Cotrufo et al., 2013). These microbial inputs, therefore, promote stable SOC through aggregation and mineral binding.

Although root exudates have been shown to contribute to the stabilized bulk SOC pool, exudates can also act to prime the microbial community which can stimulate degradation of organic matter (Kuzyakov, 2002; Lewis et al., 2014). However, our data suggest ecosystem properties (e.g. inundation) serve to further stabilize SOC, preventing priming and enhanced degradation. As stated previously, we determined a turnover time of 62 ± 0.09 years for the open

mangrove site and 103 ± 0.91 years for the confined mangrove site. This variation in turnover time between sites indicates differences in the timescale of carbon storage are the result of site-specific differences in SOC stability due to variability in tidal flushing. Stability differences between sites were evident in $(Ad/Al)_v$ ratios and activation energy distributions. Lower $(Ad/Al)_v$ ratios indicated organic matter from the confined mangrove site was more stable than organic matter from the open mangrove site (Figure 9). This trend was further supported by activation energy distributions, with the confined mangrove site having a significantly higher mean peak activation energy than the open mangrove site ($p < 0.05$) and therefore more stable SOC (Figure 9) (Hemingway et al., 2017).

The trends in stability are reflective of the tidal influences at each site. The open mangrove site

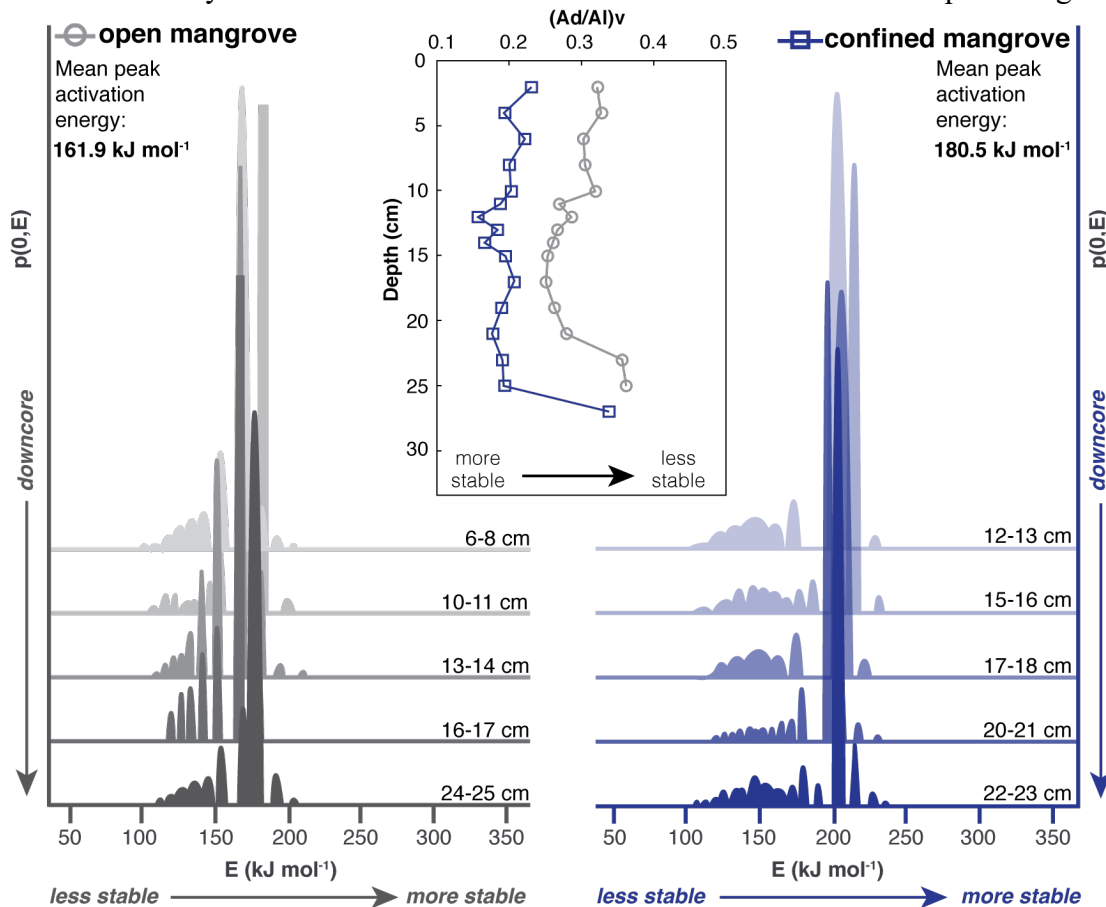


Figure 9 Downcore activation energy distributions and $(Ad/Al)_v$ profiles from the open and confined mangrove sites. Both show no change in stability down core. Overall, the confined mangrove site has more stable soil organic carbon (SOC) as evidenced by a higher mean peak activation energy and lower $(Ad/Al)_v$ ratios.

receives daily tidal flushing which introduces oxygen to the system, creating conditions more conducive to organic matter degradation. The soil at the confined mangrove site is water-logged and rarely flushed, creating continual anoxic conditions, that favor the preservation of organic matter.

Figure 10 highlights the mechanisms responsible for carbon stabilization at our sites. The driver of SOC stability is the microbial processing of root exudates, while inundation only serves to enhance SOC stability, rather than drive it. Mangrove peats experiencing regular tidal flushing can expect turnover times of a timescale similar to that of the open mangrove site (~62 years). Inundation at the confined mangrove site serves to prevent microbial priming and inhibit degradation which is reflected in a longer turnover time.

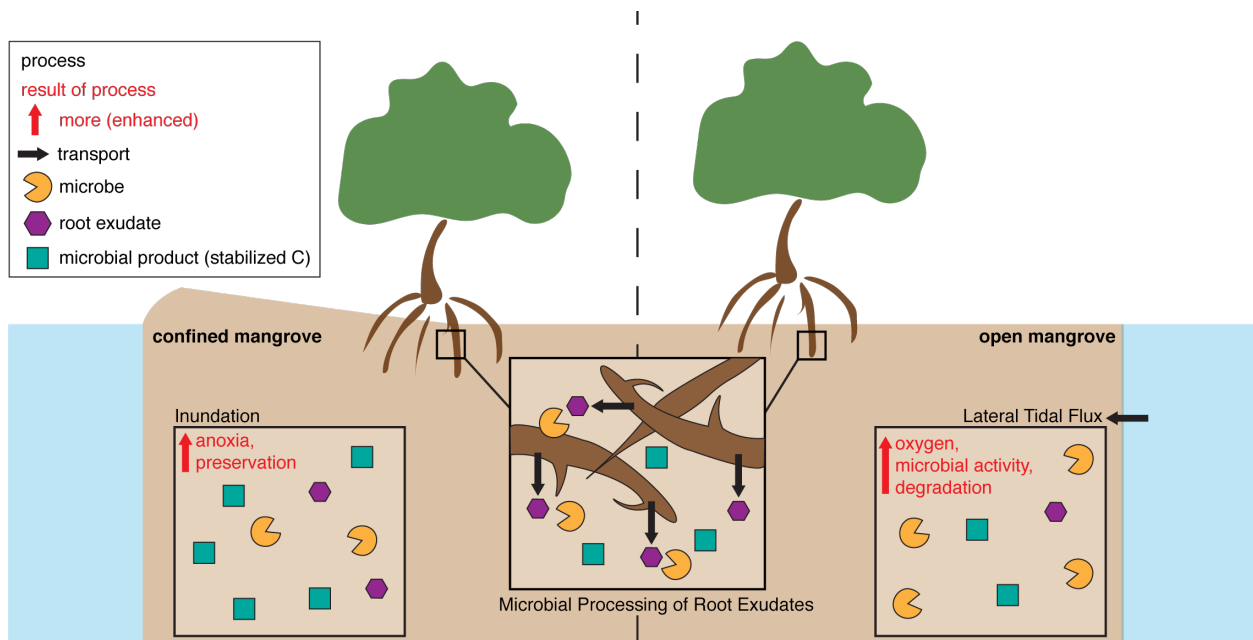


Figure 10 Conceptual diagram describing soil organic carbon (SOC) cycling and stabilization at the open and confined mangrove sites. SOC, sourced from root exudates, is ultimately stabilized through microbial processing while inundation serves to further stabilize SOC.

Mangrove forests are extremely efficient natural carbon sinks (McLeod et al., 2011). Here, we show mangrove bulk SOC is made up of young ($F_m > 1$), relatively stable carbon, sourced

from root exudates, which can be transported in pore waters to a depth of at least 32 cm. Although root exudates are generally thought to cycle quickly, microbial processing can act to stabilize them and provide a pathway for incorporation into bulk SOC. Differences in tidal flushing at our two study sites (open and confined mangrove) were shown to further contribute to stability, with soil inundation at the confined mangrove site enhancing SOC stability.

The impact climate change will have on *in situ* carbon cycling and stability processes is uncertain (Macreadie et al., 2019). Currently, there is a paucity of data on the potentially important role root exudates play in the long-term storage of mangrove SOC and how the release of exudates will be impacted by increased temperatures and carbon dioxide levels. Previous research in upland terrestrial and marsh habitats have shown increased temperatures and dioxide levels to be positively correlated with the increased release of root exudates (Bardgett, 2011; Zhai et al., 2013); however, these systems are governed by different hydrodynamics and biogeochemical parameters. The processes we identify in this paper contribute to the efficiency of the mangrove carbon sink and disruptions may impact the future efficacy of the sink.

Chapter 4. Conclusions

The most recent Intergovernmental Panel on Climate Change (IPCC) report laid out a bleak vision of the future. Human activities have increased global temperatures approximately 1°C since the industrial revolution and have risen at a rate of 0.1-0.3°C per decade over the last twenty years (Allen et al., 2018). Increased greenhouse gas emissions are the main contributor to rising global temperatures. The IPCC has emphasized the need to not only reduce carbon emissions, but also actively remove CO₂ from the atmosphere (Allen et al., 2018).

One natural way to mitigate the emission of CO₂ involves the afforestation and reforestation of terrestrial and coastal areas, and the protection of existing vegetation-associated carbon stocks (Canadell and Raupach, 2008). Coastal wetlands, including mangroves, sequester significantly more carbon per unit area than terrestrial forests, making their protection and reforestation a logical focus for climate remediation efforts (Alongi, 2014). However, the fate of mangrove carbon stocks remains uncertain in the face of a changing climate and rising sea levels (Jones et al., 2019; Lewis et al., 2014; Macreadie et al., 2019; Rogers et al., 2019).

This research provides a greater understanding of the mechanisms governing carbon cycling and stabilization in mangrove ecosystems. The combined use of ²¹⁰Pb and ¹⁴C chronologies revealed a previously unrecognized carbon transport mechanism, whereby young carbon is transported to deeper soil layers and stabilized. We argue this young carbon is sourced from root exudates and ultimately stabilized as a result of microbially processing.

We have also provided one of the first determinations of turnover time in a mangrove soil. Both study sites displayed turnover times > 50 years, despite the influence of active microbial

processing. The ability of these systems to pump young carbon to depth and store it for long periods of time suggests mangroves are more effective at sequestering carbon than previously thought. However, the differences in turnover time between sites can be attributed to site-specific variation in tidal influence. Lignin phenol ratios and activation energy distributions indicated inundation served to further stabilize microbially-processed carbon, while tidal flushing introduced oxygen to the system and stimulated microbial activity.

The multi-proxy approach taken here which utilized a variety of chronometers (^{210}Pb , ^{137}Cs , ^{14}C), source-specific tracers (C:N ratios, $\delta^{13}\text{C}$), and measurements of stability (activation energy distributions, $(\text{Ad}/\text{Al})_v$ ratios) provides a holistic understanding of carbon cycling and stabilization within an ecosystem. However, additional work must be done to determine whether sea level rise and changing species distributions will disrupt the existing mechanisms of carbon transport and stabilization. In addition, a similar research approach should be applied to salt marsh settings and mangroves across the globe to determine whether the trends seen at these sites are universal.

References

- Abril, J.M., 2004. Constraints on the use of ^{137}Cs as a time-marker to support CRS and SIT chronologies. *Environ. Pollut.* 129, 31–37.
- Allen, M.R., Dube, O.P., Solecki, W., Aragón-Durand, F., Cramer, W., Humphreys, S., Kainuma, M., Kala, J., Mahowald, N., Mulugetta, Y., Perez, R., Wairiu, M., Zickfeld, K., 2018. Global Warming of 1.5°C. An IPCC Special Report on the impacts of global warming of 1.5°C above pre-industrial levels and related global greenhouse gas emission pathways, in the context of strengthening the global response to the to the threat of climate.
- Alongi, D.M., 2014. Carbon Cycling and Storage in Mangrove Forests. *Ann. Rev. Mar. Sci.* 6, 195–219.
- Appleby, P.G., Oldfield, F., 1978. The calculation of lead-210 dates assuming a constant rate of supply of unsupported ^{210}Pb to the sediment. *Catena* 5, 1–8.
- Bao, R., Blattmann, T.M., McIntyre, C., Zhao, M., Eglinton, T.I., 2019. Relationships between grain size and organic carbon ^{14}C heterogeneity in continental margin sediments. *Earth Planet. Sci. Lett.* 505, 76–85.
- Bao, R., McNichol, A.P., McIntyre, C.P., Xu, L., Eglinton, T.I., 2018. Dimensions of Radiocarbon Variability within Sedimentary Organic Matter. *Radiocarbon* 60, 775–790.
- Bardgett, R.D., 2011. Plant–soil interactions in a changing world. *F1000 Biol. Rep.* 3.
- Bouillon, S., Borges, A. V., Castañeda-Moya, E., Diele, K., Dittmar, T., Duke, N.C., Kristensen, E., Lee, S.Y., Marchand, C., Middelburg, J.J., Rivera-Monroy, V.H., Smith, T.J., Twilley, R.R., 2008. Mangrove production and carbon sinks: A revision of global budget estimates. *Global Biogeochem. Cycles* 22.
- Bouillon, S., Dahdouh-Guebas, F., Rao, A.V.V.S., Koedam, N., Dehairs, F., 2003. Sources of organic carbon in mangrove sediments: variability and possible ecological implications. *Hydrobiologia* 495, 33–39.
- Breithaupt, J.L., Smoak, J.M., Bianchi, T.S., Vaughn, D., Sanders, C.J., Radabaugh, K.R., Osland, M.J., Feher, L.C., Lynch, J.C., Cahoon, D.R., Anderson, G.H., Whelan, K.R.T., Rosenheim, B.E., Moyer, R.P., Chambers, L.G., 2020. Increasing rates of carbon burial in southwest Florida coastal wetlands, *Journal of Geophysical Research: Biogeosciences*.
- Breithaupt, J.L., Smoak, J.M., Byrne, R.H., Waters, M.N., Moyer, R.P., Sanders, C.J., 2018. Avoiding timescale bias in assessments of coastal wetland vertical change. *Limnol. Oceanogr.* 63, 477–495.
- Breithaupt, J.L., Smoak, J.M., Smith, T.J., Sanders, C.J., 2014. Temporal variability of carbon and nutrient burial, sediment accretion, and mass accumulation over the past century in a carbonate platform mangrove forest of the Florida Everglades. *J. Geophys. Res. Biogeosciences* 119, 2032–2048.
- Breithaupt, J.L., Smoak, J.M., Smith, T.J., Sanders, C.J., Hoare, A., 2012. Organic carbon burial rates in mangrove sediments: Strengthening the global budget. *Global Biogeochem. Cycles* 26.
- Canadell, J.G., Raupach, M.R., 2008. Managing forests for climate change mitigation. *Science* 320, 1456–1457.

- Carpenter, R., 1997. Interactions of Radionuclides with Sediments and Suspended Particles Ch. 4. International Atomic Energy Agency, Vienna.
- Chen, R., Twilley, R.R., 1999. A simulation model of organic matter and nutrient accumulation in mangrove wetland soils. *Biogeochemistry* 44, 93–118.
- Chmura, G.L., Anisfeld, S.C., Cahoon, D.R., Lynch, J.C., 2003. Global carbon sequestration in tidal, saline wetland soils. *Global Biogeochem. Cycles* 17.
- Cotrufo, M.F., Wallenstein, M.D., Boot, C.M., Deneff, K., Paul, E., 2013. The Microbial Efficiency-Matrix Stabilization (MEMS) framework integrates plant litter decomposition with soil organic matter stabilization: Do labile plant inputs form stable soil organic matter? *Glob. Chang. Biol.* 19, 988–995.
- Derrien, D., Marol, C., Balesdent, J., 2004. The dynamics of neutral sugars in the rhizosphere of wheat. An approach by ^{13}C pulse-labelling and GC/C/IRMS. *Plant Soil* 267, 243–253.
- Dixon, R.K., Krankina, O.N., 1995. Can the Terrestrial Biosphere Be Managed to Conserve and Sequester Carbon?, in: *Carbon Sequestration in the Biosphere*. Springer Berlin Heidelberg, Berlin, Heidelberg, pp. 153–179.
- Donato, D.C., Kauffman, J.B., Murdiyarso, D., Kurnianto, S., Stidham, M., Kanninen, M., 2011. Mangroves among the most carbon-rich forests in the tropics. *Nat. Geosci.* 4, 293–297.
- Doughty, C.L., Langley, J.A., Walker, W.S., Feller, I.C., Schaub, R., Chapman, S.K., 2016. Mangrove Range Expansion Rapidly Increases Coastal Wetland Carbon Storage. *Estuaries and Coasts* 39, 385–396.
- Drexler, J.Z., Fuller, C.C., Archfield, S., 2018. The approaching obsolescence of ^{137}Cs dating of wetland soils in North America. *Quat. Sci. Rev.* 199, 83–96.
- Duarte, C.M., Cebrián, J., 1996. The fate of marine autotrophic production. *Limnol. Oceanogr.* 41, 1758–1766.
- Ertel, J.R., Hedges, J.I., 1984. The lignin component of humic substances: Distribution among soil and sedimentary humic, fulvic, and base-insoluble fractions. *Geochim. Cosmochim. Acta* 48, 2065–2074.
- Fernandez, A., Santos, G.M., Williams, E.K., Pendergraft, M.A., Vetter, L., Rosenheim, B.E., 2014. Blank Corrections for Ramped Pyrolysis Radiocarbon Dating of Sedimentary and Soil Organic Carbon. *Anal. Chem.* 86, 12085–12092.
- Giri, C., Ochieng, E., Tieszen, L.L., Zhu, Z., Singh, A., Loveland, T., Masek, J., Duke, N., 2011. Status and distribution of mangrove forests of the world using earth observation satellite data. *Glob. Ecol. Biogeogr.* 20, 154–159.
- Gross, C.D., Harrison, R.B., 2019. The Case for Digging Deeper: Soil Organic Carbon Storage, Dynamics, and Controls in Our Changing World. *Soil Syst.* 3.
- He, Q., Walling, D.E., 1997. The distribution of fallout ^{137}Cs and ^{210}Pb in undisturbed and cultivated soils. *Appl. Radiat. Isot.* 48, 677–690.
- Hedges, J.I., Ertel, J.R., 1982. Characterization of lignin by gas capillary chromatography of cupric oxide oxidation products. *Anal. Chem.* 54, 174–178.
- Hedges, J.I., Mann, D.C., 1979. The characterization of plant tissues by their lignin oxidation products. *Geochim. Cosmochim. Acta* 43, 1803–1807.
- Hemingway, J.D., 2016. rampedpyrox: open-source tools for thermoanalytical data analysis. <http://pypi.python.org/pypi/rampedpyrox>.
- Hemingway, J.D., Rothman, D.H., Grant, K.E., Rosengard, S.Z., Eglinton, T.I., Derry, L.A., Galy, V. V., 2019. Mineral protection regulates long-term global preservation of natural organic carbon. *Nature* 570, 228–231.

- Hemingway, J.D., Rothman, D.H., Rosengard, S.Z., Galy, V. V., 2017. Technical note: An inverse method to relate organic carbon reactivity to isotope composition from serial oxidation. *Biogeosciences* 14, 5099–5114.
- Jenkinson, D.S., Rayner, J.H., 1977. The Turnover of Soil Organic Matter in some of the Rothamsted Classical Experiments. *Soil Sci.* 123, 298–305.
- Jones, M.C., Wingard, G.L., Stackhouse, B., Keller, K., Willard, D., Marot, M., Landacre, B., E. Bernhardt, C., 2019. Rapid inundation of southern Florida coastline despite low relative sea-level rise rates during the late-Holocene. *Nat. Commun.* 10.
- Kramer, C., Trumbore, S., Fröberg, M., Cisneros Dozal, L.M., Zhang, D., Xu, X., Santos, G.M., Hanson, P.J., 2010. Recent (<4 year old) leaf litter is not a major source of microbial carbon in a temperate forest mineral soil. *Soil Biol. Biochem.* 42, 1028–1037.
- Krauss, K.W., From, A.S., Doyle, T.W., Doyle, T.J., Barry, M.J., 2011. Sea-level rise and landscape change influence mangrove encroachment onto marsh in the Ten Thousand Islands region of Florida, USA. *J. Coast. Conserv.* 15, 629–638.
- Kristensen, E., Bouillon, S., Dittmar, T., Marchand, C., 2008. Organic carbon dynamics in mangrove ecosystems: A review. *Aquat. Bot.* 89, 201–219.
- Kuzyakov, Y., 2002. Review: Factors affecting rhizosphere priming effects. *J. Plant Nutr. Soil Sci.* 165, 382–396.
- Lehmann, J., Kleber, M., 2015. The contentious nature of soil organic matter. *Nature* 528, 60–68.
- Lewis, D.B., Brown, J.A., Jimenez, K.L., 2014. Effects of flooding and warming on soil organic matter mineralization in *Avicennia germinans* mangrove forests and *Juncus roemerianus* salt marshes. *Estuar. Coast. Shelf Sci.* 139, 11–19.
- Louchouart, P., Amon, R.M.W., Duan, S., Pondell, C., Seward, S.M., White, N., 2010. Analysis of lignin-derived phenols in standard reference materials and ocean dissolved organic matter by gas chromatography/tandem mass spectrometry. *Mar. Chem.* 118, 85–97.
- Macreadie, P.I., Anton, A., Raven, J.A., Beaumont, N., Connolly, R.M., Friess, D.A., Kelleway, J.J., Kennedy, H., Kuwae, T., Lavery, P.S., Lovelock, C.E., Smale, D.A., Apostolaki, E.T., Atwood, T.B., Baldock, J., Bianchi, T.S., Chmura, G.L., Eyre, B.D., Fourqurean, J.W., Hall-Spencer, J.M., Huxham, M., Hendriks, I.E., Krause-Jensen, D., Laffoley, D., Luisetti, T., Marbà, N., Masque, P., McGlathery, K.J., Megonigal, J.P., Murdiyarso, D., Russell, B.D., Santos, R., Serrano, O., Silliman, B.R., Watanabe, K., Duarte, C.M., 2019. The future of Blue Carbon science. *Nat. Commun.* 10.
- Maher, D.T., Santos, I.R., Golsby-Smith, L., Gleeson, J., Eyre, B.D., 2013. Groundwater-derived dissolved inorganic and organic carbon exports from a mangrove tidal creek: The missing mangrove carbon sink? *Limnol. Oceanogr.* 58, 475–488.
- Marchio, D., Savarese, M., Bovard, B., Mitsch, W., Marchio, D.A., Savarese, M., Bovard, B., Mitsch, W.J., 2016. Carbon Sequestration and Sedimentation in Mangrove Swamps Influenced by Hydrogeomorphic Conditions and Urbanization in Southwest Florida. *Forests* 7.
- McCraith, B.J., Gardner, L.R., Wetthey, D.S., Moore, W.S., 2003. The effect of fiddler crab burrowing on sediment mixing and radionuclide profiles along a topographic gradient in a southeastern salt marsh. *J. Mar. Res.* 61, 359–390.
- McLeod, E., Chmura, G.L., Bouillon, S., Salm, R., Björk, M., Duarte, C.M., Lovelock, C.E., Schlesinger, W.H., Silliman, B.R., 2011. A blueprint for blue carbon: toward an improved understanding of the role of vegetated coastal habitats in sequestering CO₂. *Front. Ecol. Environ.* 9, 552–560.

- Morris, K., Butterworth, J.C., Livens, F.R., 2000. Evidence for the Remobilization of Sellafield Waste Radionuclides in an Intertidal Salt Marsh, West Cumbria, U.K. *Estuar. Coast. Shelf Sci.* 51, 613–625.
- NOAA, 2019. NOAA Tides & Currents [WWW Document]. *Relat. Sea Lev. Trend* 87248580 Key West, Florida.
- Ouyang, X., Lee, S.Y., Connolly, R.M., 2017. The role of root decomposition in global mangrove and saltmarsh carbon budgets. *Earth-Science Rev.* 166, 53–63.
- Plante, A.F., Beupré, S.R., Roberts, M.L., Baisden, T., 2013. Distribution of Radiocarbon Ages in Soil Organic Matter by Thermal Fractionation. *Radiocarbon* 55, 1077–1083.
- Rasse, D.P., Rumpel, C., Dignac, M.-F., 2005. Is soil carbon mostly root carbon? Mechanisms for a specific stabilisation. *Plant Soil* 269, 341–356.
- Reimer, R., Reimer, P., 2017. CALIBomb.
- Rogers, K., Kelleway, J.J., Saintilan, N., Megonigal, J.P., Adams, J.B., Holmquist, J.R., Lu, M., Schile-Beers, L., Zawadzki, A., Mazumder, D., Woodroffe, C.D., 2019. Wetland carbon storage controlled by millennial-scale variation in relative sea-level rise. *Nature* 567, 91–95.
- Rosenheim, B.E., Day, M.B., Domack, E., Schrum, H., Benthien, A., Hayes, J.M., 2008. Antarctic sediment chronology by programmed-temperature pyrolysis: Methodology and data treatment. *Geochemistry Geophys. Geosystems* 9.
- Rosenheim, B.E., Galy, V., 2012. Direct measurement of riverine particulate organic carbon age structure. *Geophys. Res. Lett.* 39, 1–6.
- Saintilan, N., Wilson, N.C., Rogers, K., Rajkaran, A., Krauss, K.W., 2014. Mangrove expansion and salt marsh decline at mangrove poleward limits. *Glob. Chang. Biol.* 20, 147–157.
- Sanderman, J., Baldock, J.A., Amundson, R., 2008. Dissolved organic carbon chemistry and dynamics in contrasting forest and grassland soils. *Biogeochemistry* 89, 181–198.
- Schmidt, M.W.I., Torn, M.S., Abiven, S., Dittmar, T., Guggenberger, G., Janssens, I.A., Kleber, M., Kögel-Knabner, I., Lehmann, J., Manning, D.A.C., Nannipieri, P., Rasse, D.P., Weiner, S., Trumbore, S.E., 2011. Persistence of soil organic matter as an ecosystem property. *Nature* 478, 49–56.
- Shier, D.E., 1969. Vermetid Reefs and Coastal Development in the Ten Thousand Islands, Southwest Florida. *GSA Bull.* 80, 485–508.
- Sierra, C.A., Müller, M., Metzler, H., Manzoni, S., Trumbore, S.E., 2017. The muddle of ages, turnover, transit, and residence times in the carbon cycle. *Glob. Chang. Biol.* 23, 1763–1773.
- Simpson, L.T., Osborne, T.Z., Duckett, L.J., Feller, I.C., 2017. Carbon Storages along a Climate Induced Coastal Wetland Gradient. *Wetlands* 37, 1023–1035.
- Smoak, J.M., Breithaupt, J.L., Smith, T.J., Sanders, C.J., 2013. Sediment accretion and organic carbon burial relative to sea-level rise and storm events in two mangrove forests in Everglades National Park. *Catena* 104, 58–66.
- Steinmuller, H.E., Chambers, L.G., 2019. Characterization of coastal wetland soil organic matter: Implications for wetland submergence. *Sci. Total Environ.* 677, 648–659.
- Stuiver, M., Reimer, P.J., Reimer, R.W., 2019. CALIB Radiocarbon Calibration.
- Torn, M.S., Swanston, C.W., Castanha, C., Trumbore, S.E., 2009. Storage and turnover of organic matter in soil.
- Townsend, A.R., Vitousek, P.M., Trumbore, S.E., 1995. Soil Organic Matter Dynamics Along Gradients in Temperature and Land Use on the Island of Hawaii. *Ecology* 76, 721–733.
- Trumbore, S., 2009. Radiocarbon and Soil Carbon Dynamics. *Annu. Rev. Earth Planet. Sci.* 37,

47–66.

- Trumbore, S., 2000. Age of Soil Organic Matter and Soil Respiration: Radiocarbon Constraints on Belowground C Dynamics. *Ecol. Appl.* 10, 399–411.
- Trumbore, S.E., Vogel, J.S., Southon, J.R., 1989. AMS ¹⁴C Measurements of Fractionated Soil Organic Matter: An Approach to Deciphering the Soil Carbon Cycle. *Radiocarbon* 31, 644–654.
- Van de Broek, M., Vandendriessche, C., Poppelmonde, D., Merckx, R., Temmerman, S., Govers, G., 2018. Long-term organic carbon sequestration in tidal marsh sediments is dominated by old-aged allochthonous inputs in a macrotidal estuary. *Glob. Chang. Biol.* 24, 2498–2512.
- Van Hees, P.A.W., Jones, D.L., Finlay, R., Godbold, D.L., Lundström, U.S., 2005. The carbon we do not see - The impact of low molecular weight compounds on carbon dynamics and respiration in forest soils: A review. *Soil Biol. Biochem.* 37, 1–13.
- Vetter, L., Rosenheim, B.E., Fernandez, A., Törnqvist, T.E., 2017. Short organic carbon turnover time and narrow ¹⁴C age spectra in early Holocene wetland paleosols. *Geochemistry, Geophys. Geosystems* 18, 142–155.
- Williams, E.K., Rosenheim, B.E., 2015. What happens to soil organic carbon as coastal marsh ecosystems change in response to increasing salinity? An exploration using ramped pyrolysis. *Geochemistry, Geophys. Geosystems* 16, 2322–2335.
- Woodroffe, C.D., Rogers, K., McKee, K.L., Lovelock, C.E., Mendelssohn, I.A., Saintilan, N., 2016. Mangrove Sedimentation and Response to Relative Sea-Level Rise. *Ann. Rev. Mar. Sci.* 8, 243–266.
- Yao, Q., Liu, K., 2017. Dynamics of marsh-mangrove ecotone since the mid-Holocene: A palynological study of mangrove encroachment and sea level rise in the Shark River Estuary, Florida. *PLoS One* 12.
- Zhai, X., Piwpuan, N., Arias, C.A., Headley, T., Brix, H., 2013. Can root exudates from emergent wetland plants fuel denitrification in subsurface flow constructed wetland systems? *Ecol. Eng.* 61, 555–563.
- Zieman, Jr., J.C., 1972. Origin of Circular Beds of *Thalassia* (Spermatophyta: Hydrocharitaceae) in South Biscayne Bay, Florida, and their Relationship to Mangrove Hammocks. *Bull. Mar. Sci.* 22, 559–574.

Appendix A: Supplementary Information for Chapter Three

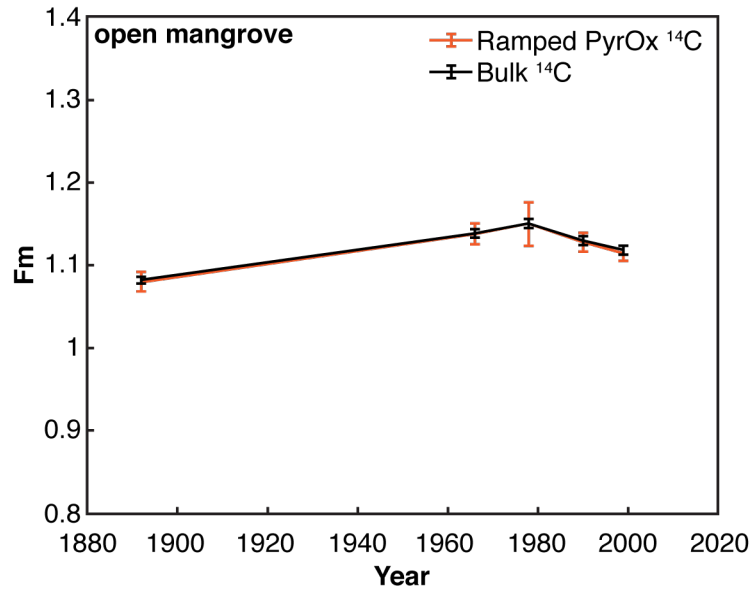


Figure 1A Comparison of radiocarbon values (fraction modern, F_m) from Ramped PyrOx and bulk combustion from the open mangrove site. The weighted average of all Ramped PyrOx aliquots aligns with the radiocarbon signature of bulk material, indicating bulk dates accurately reflect the radiocarbon signature of the bulk soil pool.

A.1 Carbon Burial Calculations

The average mass of young ^{14}C in a single interval was scaled up to 25 cm to encompass the entirety of the ^{210}Pb dates. Total young carbon burial was then scaled up using an annual organic carbon burial rate of $123 \text{ g m}^{-2} \text{ y}^{-1}$ (Breithaupt et al., 2014) and a global mangrove area of $137,760 \text{ km}^2$ (Giri et al., 2011) and averaged between sites.

Table 1A Two end-member mixing model for the open mangrove (OM) site. Used to determine the mass of young carbon buried at each site.

Interval Name	Fraction of Young ^{14}C	Fraction of Older ^{14}C	Dry Weight (g)	% OC	Mass of OC (g)	Mass of Young ^{14}C (g)
OM 6-8 cm	0.76	0.24	0.77	0.2159	0.166	0.126
OM 10 -11 cm	0.85	0.15	0.53	0.1915	0.101	0.086
OM 13-14 cm	1.00	0	0.41	0.225	0.092	0.092
OM 16-17 cm	0.92	0.08	0.54	0.1827	0.099	0.091
OM 24-25 cm	0.55	0.45	0.83	0.1563	0.13	0.072
Average						0.081

Table 2A Two end-member mixing model for the confined mangrove (CM) site. Used to determine the mass of young carbon buried at each site.

Interval Name	Fraction of Young ^{14}C	Fraction of Older ^{14}C	Dry Weight (g)	% OC	Mass of OC (g)	Mass of Young ^{14}C (g)
CM 4-6 cm	0.52	0.48	1.4	0.2956	0.414	0.215
CM 12 -13 cm	1.00	0	0.75	0.2353	0.176	0.176
CM 15-16 cm	0.83	0.17	1.06	0.1759	0.186	0.154
CM 17-18 cm	0.47	0.53	1.31	0.155	0.203	0.096
CM 20-21 cm	0.27	0.73	2.11	0.982	2.072	0.563
CM 22-23 cm	0.10	0.90	1.57	0.1352	0.212	0.021
Average						0.186

A.2 Alternative Carbon Transport Mechanisms

We investigated bioturbation, root hair transport, leaching of humic acids, tidal flushing and interstitial carbonate dissolution as potential mechanisms for the ^{14}C signature at depth. The figures below display the data which help to disprove these mechanisms, ultimately drawing support for the idea that young carbon is sourced from root exudates that are transported in pore waters.

Bioturbation

Figure 8 displays the downcore trends in ^{210}Pb and ^{137}Cs activity, which show evidence of bioturbation (McCraith et al., 2003). The exponential decrease in ^{210}Pb activity and the distinct ^{137}Cs peaks indicate either no influence of bioturbation or constant rates of bioturbation which have not impacted ^{210}Pb and ^{137}Cs profiles.

Root Hairs

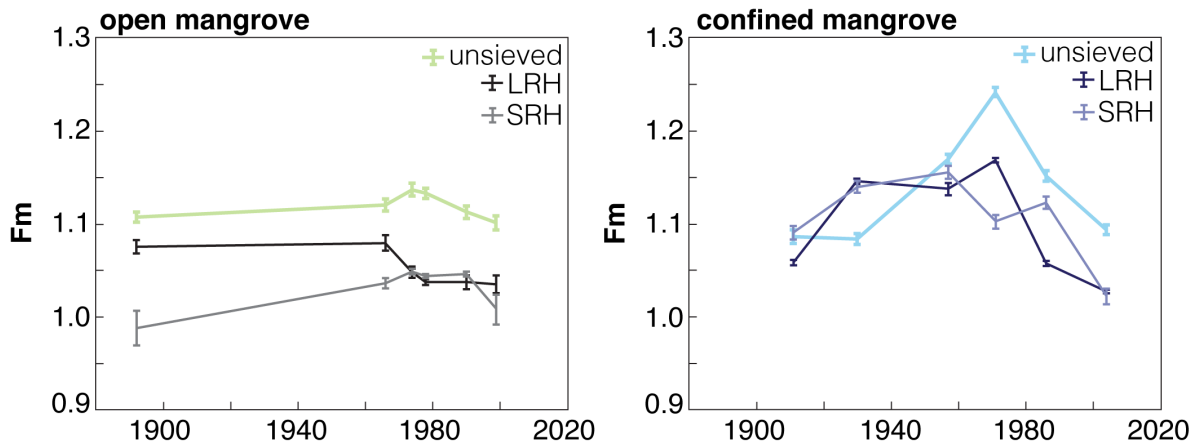


Figure 2A Radiocarbon (^{14}C) values from unsieved material and root hairs indicate root hairs were not the source of young carbon at depth. Root hairs were separated based on size to investigate the influence of size on ^{14}C content. Large root hairs (LRH) are >1 mm and small root hairs (SRH) are ≤ 1 mm. Both LRH and SRH were consistently older than bulk unsieved material, with the exception of one interval at the confined mangrove site. This indicates root hairs are not transporting young carbon to depth. Error bars incorporate standard error and ^{14}C blank correction.

Humic Acids

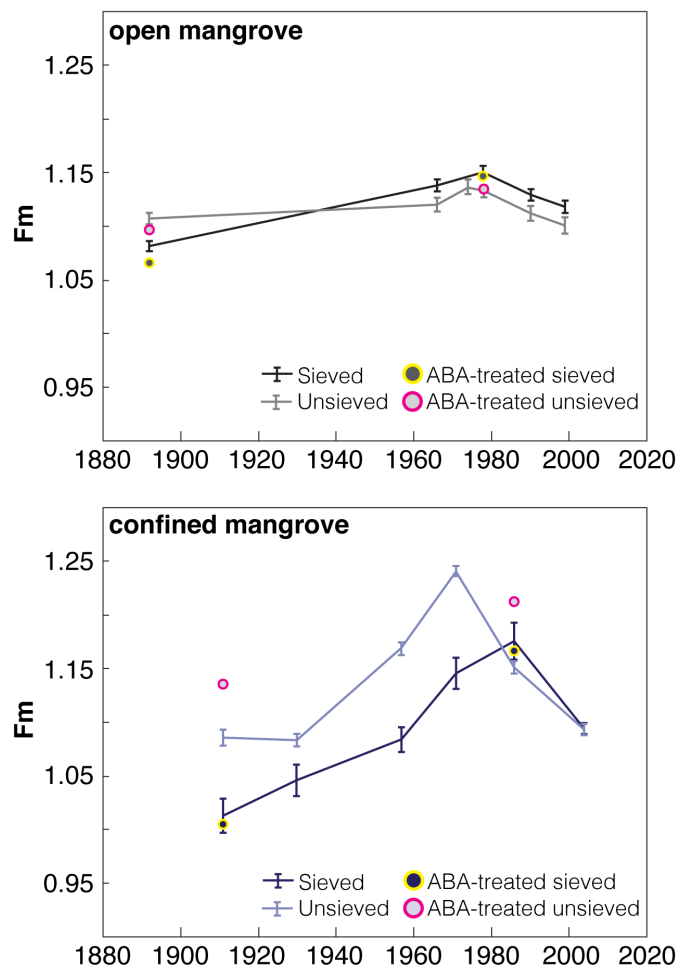


Figure 3A Comparison of radiocarbon (^{14}C) values from acid-base-acid (ABA) treated samples, sieved and unsieved samples indicates humic acids did not bias dates to be younger. Eight samples from the open and confined mangrove sites were ABA treated to test for the influence of humic acids on soil dates. Humic acids can be leached from material in low pH conditions, advect downward with pore waters and reabsorb into organic matter, biasing ^{14}C ages to be younger. ABA treatment removes humic acids, giving insight into whether organic matter is influenced by humic absorption. ^{14}C dates of ABA-treated samples (circles) revealed modern ages ($F_m > 1$) for all intervals, indicating humic acids are not the mechanism by which young carbon is being transported through the soil column. Error bars include standard error and ^{14}C blank correction

Figure 3A (Continued)

For both sites, the ^{14}C signatures of the sieved ABA-treated material aligns with the ^{14}C signatures of the sieved samples. This indicates sieving produces homogeneity within the sample that is reflected in ^{14}C signatures. For the open mangrove site, this relationship holds true for the ^{14}C content of unsieved, ABA-treated material and unsieved material. However, unsieved ABA-treated material from the confined mangrove site displays higher F_m values than the unsieved material. This indicates site-specific differences in the unsieved, bulk size fraction ($>500\ \mu\text{m}$). The higher degree of microbial activity at the open mangrove site may contribute to a more homogenized carbon pool, which is reflected in the similarity between unsieved ABA-treated and unsieved ^{14}C content. Therefore, a lower degree of degradation at the confined mangrove site leads to greater heterogeneity in soil matter and ^{14}C content.

Tidal Flushing

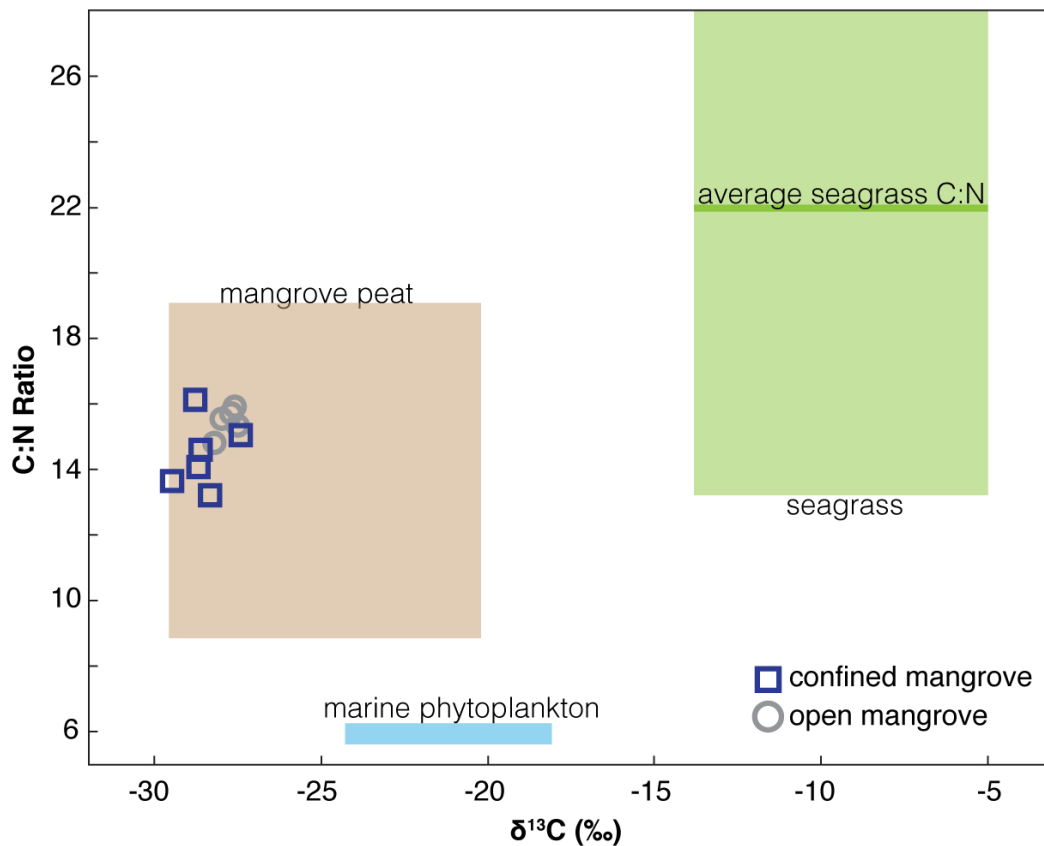


Figure 11A C:N ratios and $\delta^{13}\text{C}$ values of sieved material from the open and confined mangrove sites show no influence of marine organic matter. Values for both sites fall within the accepted C:N and $\delta^{13}\text{C}$ ranges for mangrove litter (9 to 18.8 and -29.4 to -20.6‰) (Bianchi et al. 2013; Bouillon et al. 2003). This indicates tidal flushing introduced little to no marine organic matter into the system and therefore can be discounted as the mechanism driving the downward flux of carbon.

Interstitial Carbonate Dissolution

The top 32 cm of peat from the open and confined mangrove sites contain 11.1% and 7.3% CaCO_3 , respectively (see Chapter 2) and the pH of pore waters in the area can be as low as ~ 6 , sufficient for the dissolution of calcium carbonate (Zieman, Jr., 1972). This process could create additional pore space at depth, allowing for the downward advection of pore waters and young carbon. However, due to the high porosity of mangrove peats, the creation of pore space at depth is unnecessary to explain the downward transport of young carbon.

A.3 Evidence for a Single-Pool Turnover Model

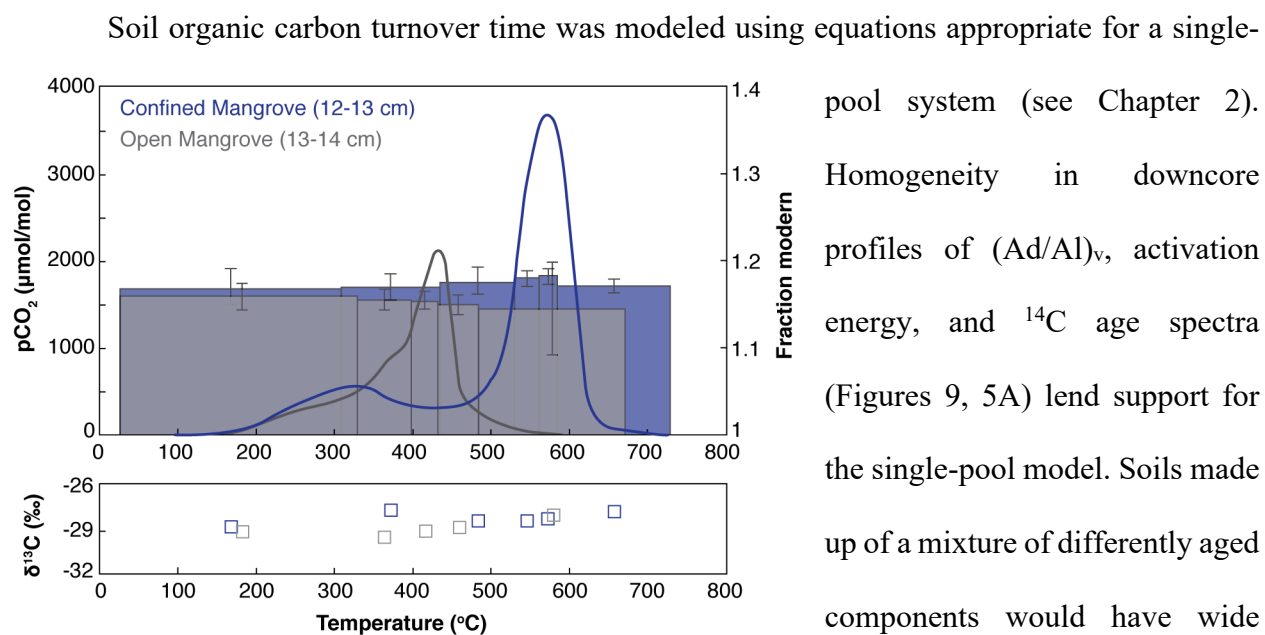


Figure 12A Thermographs from Ramped PyrOx analysis. The solid blue and gray lines show the amount of CO_2 generated during a run (left axis), while boxes represent the ages of each individual aliquot (right axis), providing a spectrum of ^{14}C ages. Age spectra indicate soil organic carbon is of similar age across the entire thermochemical spectrum. Error bars incorporate analytical error and blank corrections.

pool system (see Chapter 2). Homogeneity in downcore profiles of $(\text{Ad}/\text{Al})_v$, activation energy, and ^{14}C age spectra (Figures 9, 5A) lend support for the single-pool model. Soils made up of a mixture of differently aged components would have wide activation energy spectra, reflecting the continuum from young, labile components to older, refractory components.

Radiocarbon age spectra would show similar trends with a single soil interval containing a mixture

of young, labile carbon and older, pre-aged carbon. However, activation energy distributions and ^{14}C age spectra were largely homogeneous. Downcore homogeneity suggested mangrove soils are most accurately characterized by single turnover time, in contrast to traditional views of SOC turnover in upland terrestrial ecosystems.

Appendix B: The influence of root hairs on the isotopic composition of soil organic matter

B.1 Motivation

Wetland soil samples are traditionally sieved before analysis in order to separate soil organic matter by size fraction (Marchio et al., 2016; Van de Broek et al., 2018). Sieving also serves to remove root material which may migrate through the soil column, potentially biasing bulk soil ages. However, to the best of our understanding, few studies have investigated the ^{14}C content of mangrove root hairs and the measurable effect they may have on the age of bulk soil organic matter.

B.2 Methods

The detailed methodology related to root hair treatment can be found in Chapter 2. Root hairs were picked only from unsieved soil samples. Sieved samples contained too few root hairs for analysis, indicating sieving was successful in removing root hairs from bulk soil matter. Samples were acid treated and then divided into large root hairs (LRH) (>1 mm) and small root hairs (SRH) (≤ 1 mm) to investigate the influence of root size on SOC isotopic composition. Root hairs were then analyzed for a suite of parameters (%TOC, %N, %C, $\delta^{13}\text{C}$, ^{14}C) using elemental analysis paired with accelerator mass spectrometry.

Additionally, unsieved soil organic matter was radiocarbon dated using bulk combustion methods described in Chapter 2. These intervals were acid treated, but not sieved, to provide a more accurate comparison to root hair dates.

B.3 Results and Discussion

There were no distinct trends in root hair size or ^{14}C content at either site (Figure 1B). Both sites had three intervals where SRH were younger than LRH and three intervals where SRH were older than LRH (Table 1B). However, the bottom two intervals of the open mangrove site displayed a widening ^{14}C gap between SRH and LRH. This may reflect the more rapid movement of small roots to depth at this site.

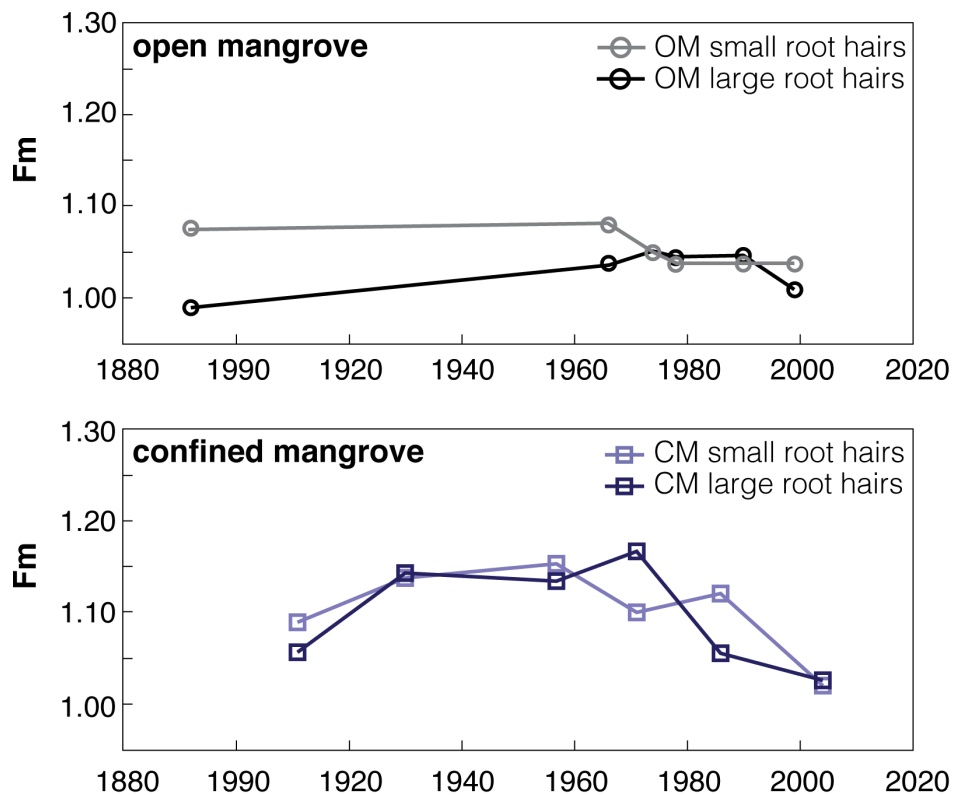


Figure 1B Radiocarbon (fraction modern, F_m) values of large and small root hairs for the open mangrove (OM) and confined mangrove (CM) sites.

Both large and small root hairs were consistently older than bulk unsieved soil ages at the open mangrove site (Table 2B). This trend held true for the confined mangrove site with the exception of both size fractions in the 20-21 cm interval and SRH for the 22-23 cm interval. The difference in ^{14}C content of root hairs and unsieved, bulk organic matter indicated root hairs were

not the source of young carbon at either site. Whereas downward root hair migration was evident, sieving served to exclude older root hair material from dated samples, rather than preventing a bias towards younger dates as previously expected. Rasse et al., (2005) found root-derived carbon had a residence time more than two times that of shoot-derived carbon, supporting the conclusion of root hairs as pathways for older carbon.

The $\delta^{13}\text{C}$ signatures of LRH at the confined mangrove site were heavier than SRH but had no consistent relationship with unsieved bulk soil $\delta^{13}\text{C}$ signatures (Figure 2B). The open mangrove

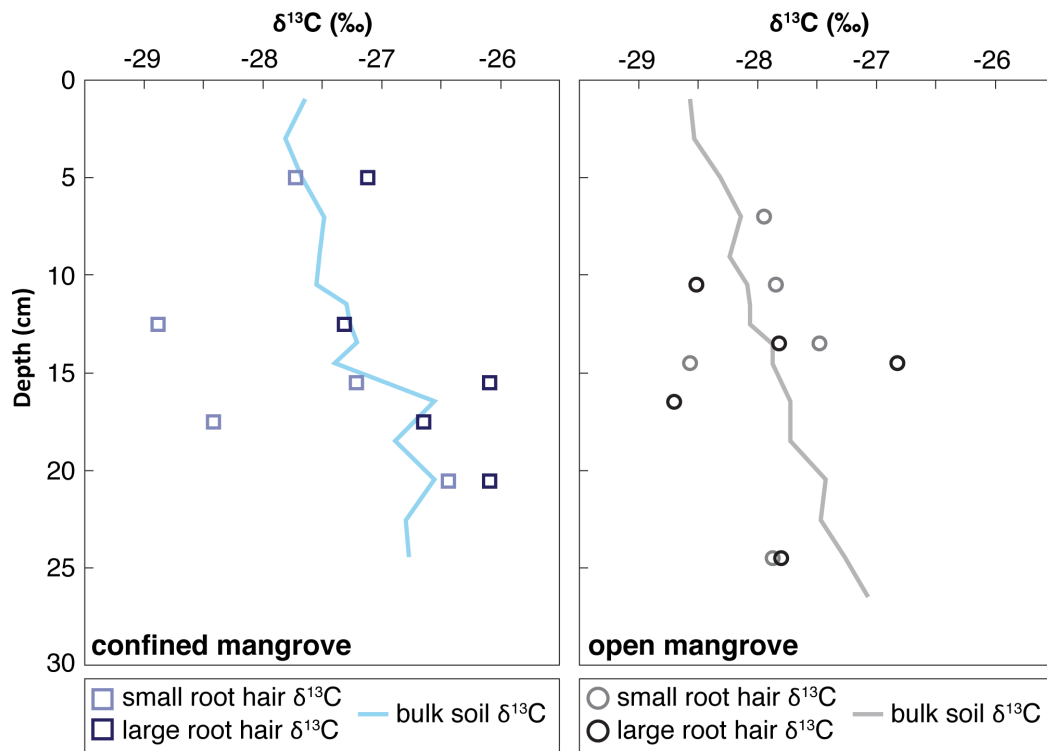


Figure 2B Downcore comparison of stable carbon isotopic data ($\delta^{13}\text{C}$) for bulk soil and root hairs.

site displayed no relationship between the $\delta^{13}\text{C}$ signatures of LRH and SRH or between root hairs and the bulk soil material (Figure 2B). However, both sites occupied a narrow isotopic range (open mangrove: -26.1‰ to -28.88‰; confined mangrove: -26.82‰ to -28.71‰). Mangrove peat falls

within this stable isotopic range, indicating soils largely retain the stable carbon isotopic signature derived from mangrove material (Bouillon et al., 2003).

A comparison of chemical parameters (%N, %C, C:N ratio) between root hairs and unsieved bulk material revealed root hairs of both size classes had higher %C and %N, resulting in lower C:N ratios than bulk material (Table 3B). These data show the significant contribution root hairs make to belowground carbon and nitrogen stocks. Previous studies have emphasized the importance of root-derived carbon for microbial communities and the large contribution roots play in global wetland carbon burial (Kramer et al., 2010; Ouyang et al., 2017).

B.4 Conclusions

The importance of roots to soil biogeochemistry has been increasingly acknowledged in the blue carbon community (Chen and Twilley, 1999; Kramer et al., 2010); however, less is known about the impact of root hairs on the ^{14}C content of bulk soil organic matter. These data provide tangible insight into root hair movement within the soil column as well as stable carbon isotopic data in line with previous findings.

Table 1B Root hair radiocarbon content (fraction modern, F_m) divided by size class, and the corresponding stable carbon isotopic signatures ($\delta^{13}\text{C}$) and ^{210}Pb ages for the open (M_o) and confined (M_c) mangrove sites. Large root hairs (LRH) are > 1 mm in length and small (SRH) are 1 mm in length. Radiocarbon values are blank corrected. F_m error includes analytical error and blank correction.

Interval	^{210}Pb Age (yr)	F_m	F_m Error	$\delta^{13}\text{C}$ (‰)
M_o (6-8 cm) LRH	1999	1.0078	0.0157	Not measured
M_o (6-8 cm) SRH	1999	1.0352	0.0095	-27.94
M_o (10-11 cm) LRH	1990	1.0464	0.0024	-28.53
M_o (10-11 cm) SRH	1990	1.0373	0.0072	-27.84
M_o (13-14 cm) LRH	1978	1.0438	0.0020	-27.82
M_o (13-14 cm) SRH	1978	1.0368	0.0023	-27.49
M_o (14-15 cm) LRH	1974	1.0490	0.0026	-26.82
M_o (14-15 cm) SRH	1974	1.0479	0.0060	-28.58

M _O (16-17 cm) LRH	1966	1.0364	0.0054	-28.71
M _O (16-17 cm) SRH	1966	1.0796	0.0082	Not measured
M _O (24-25 cm) LRH	1892	0.9880	0.0186	-27.79
M _O (24-25 cm) SRH	1892	1.0754	0.0072	-27.87
M _C (4-6 cm) LRH	2004	1.0270	0.0020	-27.12
M _C (4-6 cm) SRH	2004	1.0215	0.0079	-27.73
M _C (12-13 cm) LRH	1986	1.0570	0.0026	-27.32
M _C (12-13 cm) SRH	1986	1.1222	0.0064	-28.88
M _C (15-16 cm) LRH	1971	1.1679	0.0023	-26.1
M _C (15-16 cm) SRH	1971	1.1017	0.0071	-27.22
M _C (17-18 cm) LRH	1957	1.1370	0.0065	-26.64
M _C (17-18 cm) SRH	1957	1.1550	0.0070	-28.42
M _C (20-21 cm) LRH	1930	1.1453	0.0024	-26.10
M _C (20-21 cm) SRH	1930	1.1394	0.0062	-26.44
M _C (22-23 cm) LRH	1911	1.0581	0.0028	Not measured
M _C (22-23 cm) SRH	1911	1.0899	0.0071	Not measured

Table 2B Unsieved bulk soil organic matter radiocarbon content (fraction modern, *F_m*), and corresponding stable carbon isotopic signatures ($\delta^{13}\text{C}$) and ^{210}Pb ages for the open (*M_O*) and confined (*M_C*) mangrove sites. *M_O* (24-25 cm) and *M_C* (4-6 cm) had triplicate and duplicate samples to constrain radiocarbon content – these data were averaged when compared to root hair radiocarbon content. Radiocarbon values are blank corrected. *F_m* error includes analytical error and blank correction.

Interval	^{210}Pb Age (yr)	<i>F_m</i>	<i>F_m</i> Error	$\delta^{13}\text{C}$ (‰)
M _O (6-8 cm)	1999	1.1014	0.0076	-28.09
M _O (10-11 cm)	1990	1.1126	0.0068	-28.01
M _O (13-14 cm)	1978	1.1332	0.0055	-27.72
M _O (14-15 cm)	1974	1.1369	0.0067	-27.75
M _O (16-17 cm)	1966	1.1204	0.0065	-27.75
AVG. M _O (24-25 cm)	1892	1.1078	0.0053	-27.44
M _O (24-25 cm)	1892	1.1147	0.0051	-27.39
M _O (24-25 cm)	1892	1.1044	0.0060	-27.56
M _O (24-25 cm)	1892	1.1043	0.0048	-27.36
M _C (4-6 cm)	2004	1.0796	0.0048	-29.04
M _C (4-6 cm)	2004	1.1069	0.0045	Not measured
AVG. M _C (4-6 cm)	2004	1.0933	0.0047	-29.04
M _C (12-13 cm)	1986	1.1510	0.0056	Not measured
M _C (15-16 cm)	1971	1.2414	0.0048	Not measured
M _C (17-18 cm)	1957	1.1688	0.0055	-26.88
M _C (20-21 cm)	1930	1.0833	0.0055	-26.73
M _C (22-23 cm)	1911	1.0857	0.0073	-26.67

Table 3B Elemental analysis data (%N, %C, and C:N ratios) from two intervals at the open (M_O) and confined (M_C) mangrove sites. Unsieved soil organic matter was analyzed in addition to large root hairs (LRH) and small root hairs (SRH). Values represent averages of multiple (2-3) sample runs.

Sample	% N	% C	C:N Ratio
Unsieved M_O (6-8 cm)	1.53	30.73	20.10
M_O (6-8 cm) LRH	2.45	46.00	18.76
M_O (6-8 cm) SRH	5.16	35.89	7.43
Unsieved M_C (17-18 cm)	1.07	18.82	17.53
M_C (17-18 cm) LRH	3.16	51.08	16.27
M_C (17-18 cm) SRH	2.88	44.88	15.83

Appendix C: The impact of grain size on bulk soil organic matter radiocarbon content

C.1 Motivation

An experiment done on acid treated and filtered (<63 μm) soil samples from the open mangrove and confined mangrove sites revealed only 1-6% of the original soil interval volume was radiocarbon (^{14}C) dated. This experiment raised the question: are dates from filtered, acid treated soils representative of bulk soil organic matter? To accurately make statements about mangrove carbon cycling on an ecosystem scale, we needed to determine whether unsieved bulk material (> 500 μm) displayed similar downcore ^{14}C trends as unsieved material (e.g. Figure 7).

C.2 Methods

The full ^{14}C preparation methodology can be found in Chapter 2. In short, samples from the open and confined mangrove sites were initially sieved (<63 μm), acid treated, and prepared for ^{14}C dating using both Ramped PyrOx and bulk combustion. The same intervals were acid treated, but not sieved, and bulk combusted to compare ^{14}C content of different size fractions. Stable carbon isotopes ($\delta^{13}\text{C}$) and C:N ratios were also analyzed as tracers of environmental origin.

C.3 Results and Discussion

In general, unsieved soil organic matter displays similar trends to sieved material, with an elongated bomb curve and the transport of young carbon to depth (Figure 1C). Stable carbon

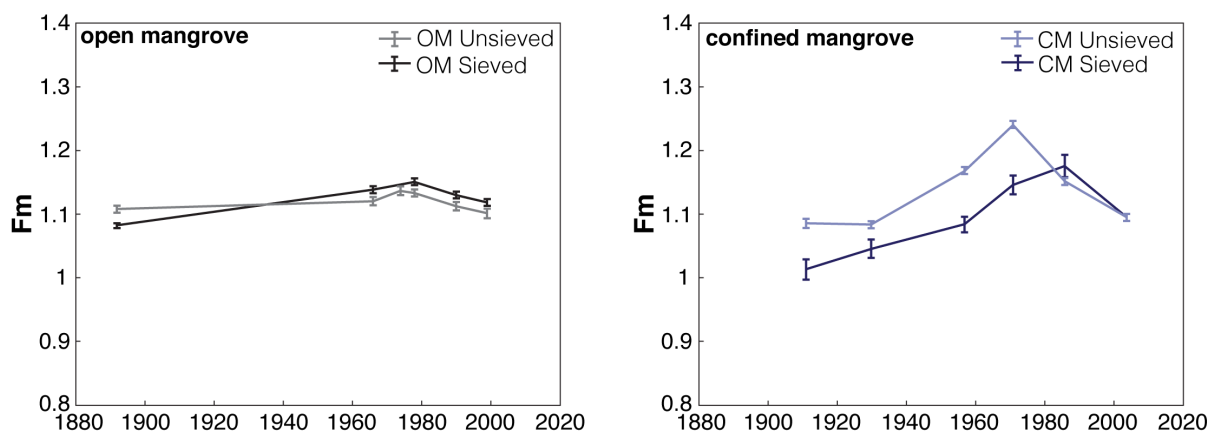


Figure 1C Radiocarbon (fraction modern, F_m) values for sieved and unsieved organic matter for the open and confined mangrove sites. Error bars factor in standard error and radiocarbon blank correction.

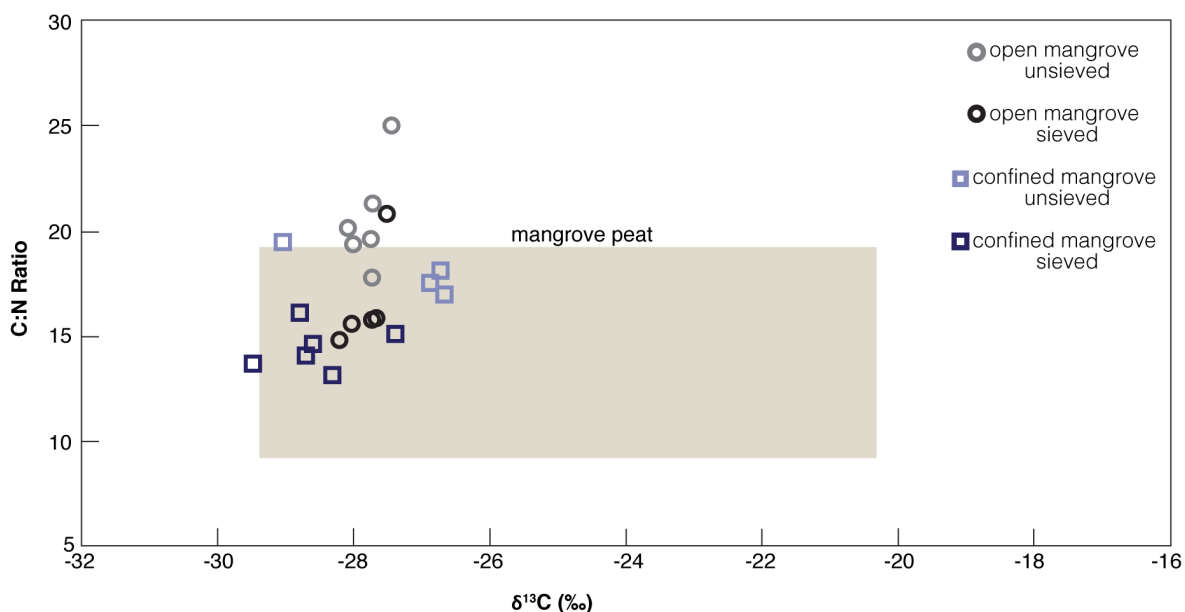


Figure 2C C:N ratios and stable carbon isotopic data (^{13}C) for sieved and unsieved material from the open and confined mangrove sites. The majority of points fall within the C:N range for mangrove litter (9-18.8) and all fall within the ^{13}C range for mangrove peat (-29.4 to -20.6‰) (Bianchi et al. 2013; Bouillon et al. 2003).

isotopic data and C:N ratios for sieved and unsieved samples were within a narrow range, indicating organic matter is largely sourced from mangrove litter (Figure 2C). These similarities in trends indicate sieved material can be used to accurately draw conclusions about the carbon

cycling within the bulk soil pool. The use of sieved material is preferred over unsieved material because it excludes potentially time transgressive material, such as roots, which have the potential to bias ages (Appendix B).

There were small differences in the downcore ^{14}C signatures of the sieved and unsieved material that suggest site-specific influences. At the open mangrove site, sieved material was consistently younger than unsieved material with the exception of open mangrove interval (24-25 cm) (Figure 1C). Previous Ramped PyrOx work has established the relationship between younger ages and smaller grain sizes in marine sediments as a result of the timescale of sediment deposition (Bao et al., 2019; Bao et al., 2018); however, because the majority of sediment deposition in mangroves autochthonous, it is not clear if this relationship applies to mangroves. The confined mangrove site showed an opposite trend with consistently older sieved material than unsieved material, except in surface intervals (Figure 1C). Activation energy distributions and (Ad/Al)_v profiles (Figure 9) indicate a higher degree of preservation at this site which may prevent the breakdown of larger, younger grain sizes. Smaller grain sizes are therefore indicative of older material which has been degraded.

Table 1C Peak ^{14}C values for open (M_O) and confined (M_C) mangrove sites divided by grain size. Due to the low resolution of ^{14}C data, possible ranges are also provided along with peak ^{14}C values which include the two points on either side of the peak. All dates are based off the ^{210}Pb chronology.

Location	Grain Size	Peak ^{14}C Values (possible peak range)
Confined Mangrove (M_C)	Unsieved (>500 μm)	1971 (1957-1986)
Confined Mangrove (M_C)	Sieved (< 63 μm)	1986 (1971-2004)
Open Mangrove (M_O)	Unsieved (>500 μm)	1974 (1966-1978)
Open Mangrove (M_O)	Sieved (< 63 μm)	1978 (1966-1990)

Post-depositional transport varied based on grain size as evidenced by offsets in ^{14}C peaks. Tidally driven pore water advection, the mechanism responsible for post-depositional ^{14}C migration, is discussed at length in Chapter 3. At both sites, sieved peaks showed a larger displacement from the interval of maximum bomb ^{14}C fallout (1963) than unsieved peaks (Table 1C). This indicates small grains more easily enter into solution and resorb onto particle surfaces.

C.4 Conclusions

This appendix demonstrated sieved material can (and should) be used to assess mangrove carbon cycling on an ecosystem-wide scale. Sieved and unsieved material displayed similar ^{14}C , C:N, and $\delta^{13}\text{C}$ trends, indicating sieved material is capturing the essential components of carbon transport. Sieving provides a safeguard against the potential introduction of migratory material, such as root hairs, that may bias dates to be older (Appendix B). However, grain size should be taken into account when assessing small-scale processes such as the mechanisms governing post-depositional ^{14}C migration.

Appendix D: Description of accretion calculations and timescale bias in Ten Thousand Islands, Florida

D.1 Motivation

Breithaupt et al., (2018) showed the use of multiple radionuclides for sediment chronology can result in differences between accretion rates due to soil and sea level processes that operate on a variety of timescales. This work highlighted a timescale bias present in the assessment of wetland vertical change inherent to the choice of chronometer. The authors suggested the use of multiple chronometers to constrain the upper and lower bounds of potential elevation change. Ten Thousand Islands (TTI) was included in the original assessment of timescale bias; however, ^{137}Cs records were omitted and ^{14}C records were taken at different sites from ^{210}Pb records. This appendix compiles ^{210}Pb , ^{137}Cs , and ^{14}C records at the open and confined mangrove sites to determine if the trends of timescale bias still hold true. We also provide an upper and lower bound of accretion for TTI. This range of accretion rates helps to fulfill the second USDA proposed objective, lending insight into coastal wetlands' ability to keep pace with SLR. Additionally, an accretion model is used to determine the impact of carbon transport on accretion rates.

D.2 Methods

Methods related to the ^{210}Pb , ^{137}Cs , and ^{14}C chronology determinations can be found in Chapter 2. Accretion rates for all radionuclides were determined by fitting linear regressions to plots of depth versus age. Radiocarbon values were calibrated using CALIB 7.1 and the IntCal13 calibration curves. These values were then used to determine a ^{14}C -based accretion rate (Stuiver

et al., 2019). Radiocarbon values used in the accretion model were calibrated using CALIBomb because soil intervals were impacted by bomb radiocarbon (i.e. $F_m > 1$) (Reimer and Reimer, 2017). The IntCal13 calibration curve was used to calibrate pre-bomb data, while the Northern Hemisphere Zone 2 (NHZ2) calibration curve was used to calibrate post-bomb data. A reservoir age was not applied to either set of radiocarbon values because stable carbon isotopic signatures indicated organic matter was largely sourced from mangrove litter (Figure 4A).

D.3 Results and Discussion

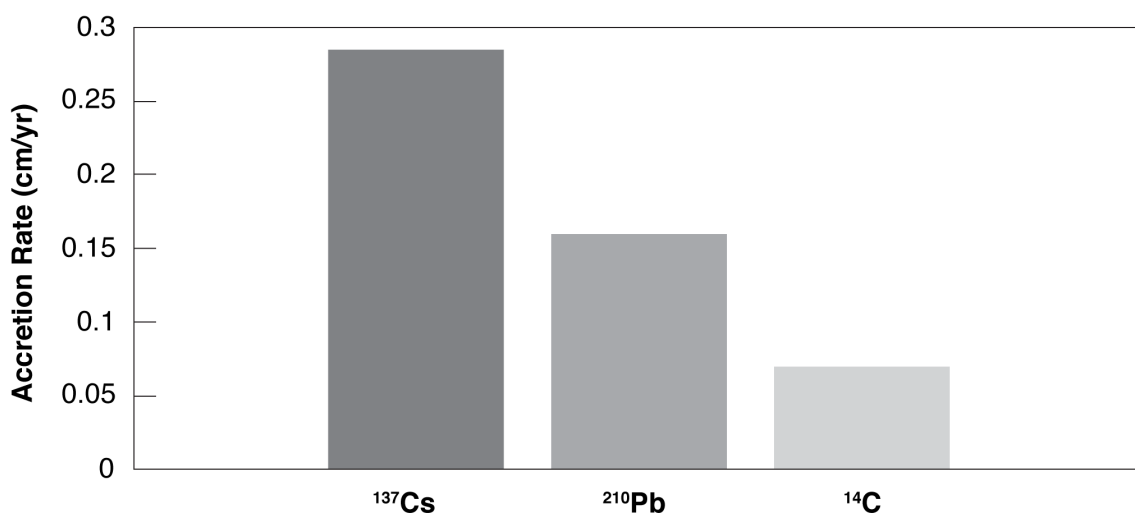


Figure 1D Accretion rates (cm/yr) for Ten Thousand Islands, Florida based on ¹³⁷Cs, ²¹⁰Pb, and ¹⁴C chronologies.

Table 1D Accretion rates (cm/yr) for the open (M_o) and confined (M_c) mangrove sites based on the depths of ^{137}Cs peaks. The accretion rate for Ten Thousand Islands (TTI) was determined by averaging the two sites.

Interval	Time Since Peak ^{137}Cs (years)	Depth of ^{137}Cs Peak	^{137}Cs Accretion Rate (cm/year)
OM (16-17 cm)	51	16.5	0.3235
CM (12-13 cm)	51	12.5	0.2451
Average TTI			0.2843

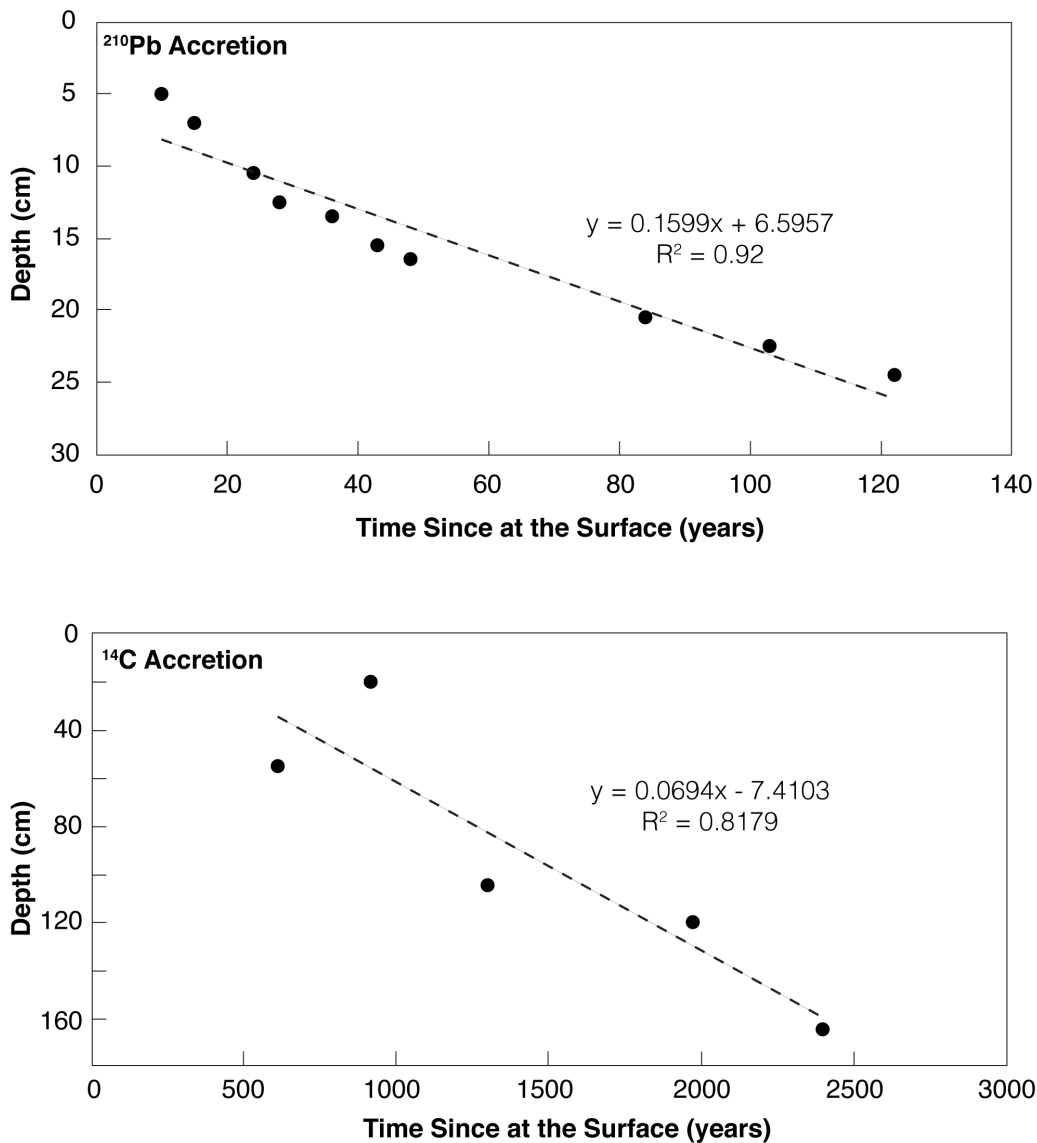


Figure 2D Ten Thousand Islands accretion rates (cm/yr) from combined open and confined mangrove ^{210}Pb and ^{14}C records. The longer ^{14}C record corresponds to a lower accretion rate of 0.0694 cm/yr. The longer ^{210}Pb record has an accretion rate of 0.1599 cm/yr. ^{14}C values were calibrated using CALIB 7.1 (Stuiver et al. 2019).

Accretion rates determined from ^{137}Cs , ^{210}Pb , and ^{14}C were all different from one another, supporting trends of timescale bias previously seen in this area (Figure 1D). The ^{137}Cs record was the shortest in length and had the highest calculated rate of accretion (Table 1D). The accretion rate determined from the ^{14}C record was the lowest and corresponded to the longest record (Figure 2D). When discussing accretion rates within the Ten Thousand Islands region, these two records should be used as the upper and lower bounds (0.0694 to 0.2843 cm/yr) to account for chronometer-based variability. Sea level at Key West, FL, the closest tide gauge to Ten Thousand Islands, has risen at a rate of 0.242 ± 0.014 cm/year since 1913 (NOAA National Ocean Service, 2019). Taking only the ^{137}Cs accretion rate into account would suggest mangroves are outpacing sea level rise, whereas the ^{14}C accretion rate suggests inundation of the coastline. The window of accretion rates determined from a suite of radionuclides provides for a better understanding of a wetland's response to sea level rise and the variability that may arise within an area.

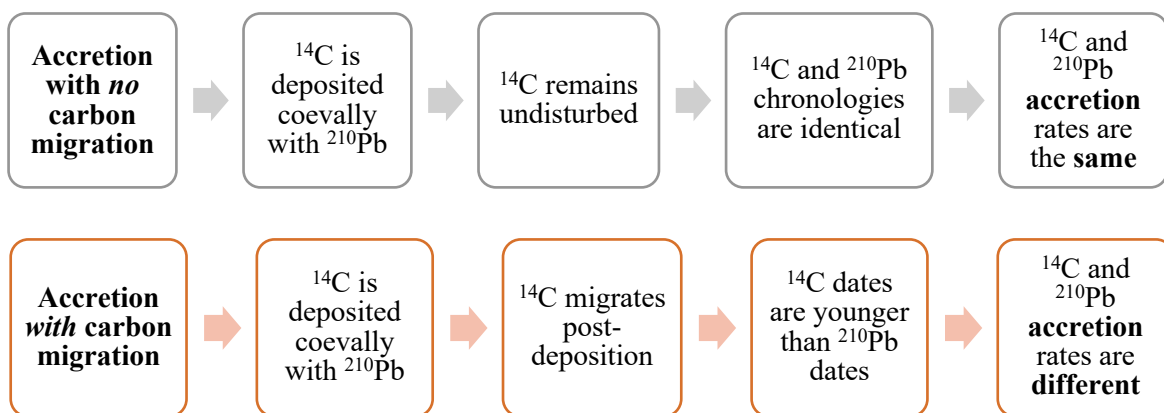


Figure 3D Conceptual diagram describing accretion modeling. In a scenario with no carbon migration, ^{14}C and ^{210}Pb accretion rates can be assumed to be the same. In a scenario with post-depositional carbon transport, ^{14}C and ^{210}Pb accretion rates will differ. With post-depositional transport, ^{14}C values must be calibrated using CALIBomb (Reimer & Reimer, 2017) because each interval has $F_m > 1$. CALIBomb returns a range of likely dates from which accretion rates can be determined.

Accretion modeling was used to understand the influence of post-depositional carbon migration on the determination of accretion rates (Figure 3D). Figure 4D displays two accretion scenarios – one for a soil column with no carbon migration (black dotted line) and the other for a soil column impacted by post-depositional carbon transport (orange dotted line). The second

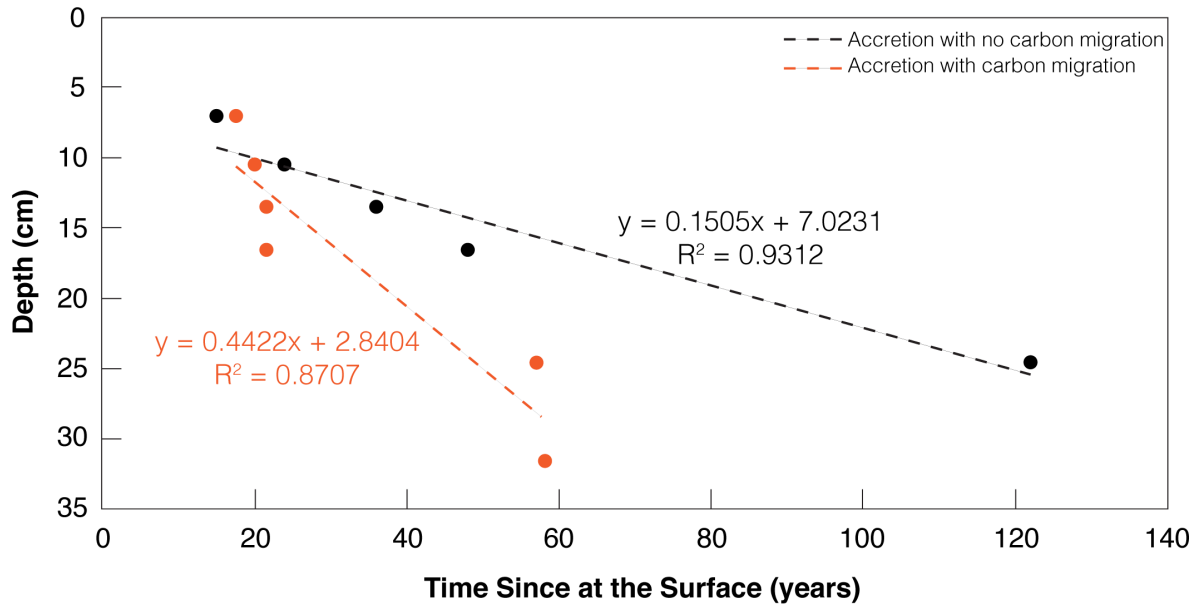


Figure 4D Modeled accretion rates (cm/yr) for the open mangrove site. Under a scenario with no post depositional carbon migration, the accretion rate would be 0.1505 cm/yr. If the ^{14}C values from the site are used to develop a chronology, where carbon transport has been observed, the resulting accretion rate is 0.4422 cm/yr. Radiocarbon values for the “accretion with carbon migration” scenario were calibrated using CALIBomb because the presence of bomb radiocarbon in samples ($F_m > 1$) (Reimer & Reimer, 2017).

scenario, accretion with carbon migration, most accurately resembles the open and confined mangrove sites. This model uses data from the open mangrove site to determine the impact of carbon migration on accretion rates. The soil column influenced by carbon transport has an accretion rate of 0.44 cm/yr compared to the accretion rate of 0.15 cm/yr from the soil column unimpacted by carbon transport. This modeling demonstrates how carbon movement can impact ^{14}C chronologies, resulting in an overestimation of the accretion rate at a site.

The presence of bomb radiocarbon was not detected below a depth of 55 cm at the open mangrove site and 42 cm at the confined mangrove site. Therefore, caution should be used when

employing ^{14}C above these depths because of its potential to skew dates and bias accretion determinations.

D.4 Conclusions

Accurate calculations of accretion rates are necessary to understand how mangrove wetlands are shifting in response to sea level rise. This appendix provides a window of accretion rates for Ten Thousand Islands, Florida which allows for a more accurate assessment of the ecosystem's ability to cope with rising sea levels. However, ^{14}C -based accretion calculations should only be used if they can be determined to be unimpacted by post-depositional carbon movement.

Appendix E: Radiocarbon and Stable Carbon Isotopic Data

Table 1E Radiocarbon (^{14}C) and stable carbon isotopic ($\delta^{13}\text{C}$) data for the open mangrove site. The open mangrove is synonymous with the UFU site code in this study. Some values were not measured, indicated by N.M.

Interval	^{14}C Prep Method	Fm Reported	Fm Reported Error	Fm Blank Corrected	Fm Error Blank Corrected	$\mu\text{mol CO}_2$	$\delta^{13}\text{C}$ (‰)
UFU1A (6-8 cm) 4A	Bulk	1.1122	0.0024	1.1184	0.0053	40.6	-28.21
UFU1A (10-11 cm) 2B	Bulk	1.1241	0.0027	1.1298	0.0051	45.8	-28.02
UFU1A (13-14 cm) 1C	Bulk	1.1447	0.0022	1.1509	0.0050	44.1	-27.73
UFU1A (16-17 cm) 2D	Bulk	1.1321	0.0026	1.1384	0.0054	41.9	-27.67
UFU1A (24-25 cm) 2A2	Bulk	1.0777	0.0022	1.0821	0.0042	52.9	-27.52
DB-1720-1 UFU1A (6-8 cm) 4A	Ramped PyrOx	1.1107	0.0024	1.1172	0.0049	20.1	-29.06
DB-1720-2 UFU1A (6-8 cm) 4A	Ramped PyrOx	1.1105	0.0021	1.1164	0.0044	22.0	-29.46
DB-1720-3 UFU1A (6-8 cm) 4A	Ramped PyrOx	1.1108	0.0021	1.1164	0.0042	23.4	-29.29
DB-1720-4 UFU1A (6-8 cm) 4A	Ramped PyrOx	1.1061	0.0022	1.1118	0.0043	22.8	-29.02
DB-1728-1 UFU1A (10-11 cm) 2B	Ramped PyrOx	1.1191	0.0030	1.1273	0.0061	16.3	N.M.
DB-1728-2 UFU1A (10-11 cm) 2B	Ramped PyrOx	1.1194	0.0023	1.1256	0.0046	21.6	-30.61
DB-1728-3 UFU1A (10-11 cm) 2B	Ramped PyrOx	1.1277	0.0023	1.1334	0.0043	23.7	-30.49
DB-1728-4 UFU1A (10-11 cm) 2B	Ramped PyrOx	1.1244	0.0026	1.1301	0.0045	23.8	-30.48
DB-1728-5 UFU1A (10-11 cm) 2B	Ramped PyrOx	1.1159	0.0025	1.1232	0.0054	18.1	-30.27
DB-1722-1 UFU1A (13-14 cm) 1C	Ramped PyrOx	1.1447	0.0024	1.1538	0.0062	15.5	-29.24

Table 1E (Continued) Radiocarbon (^{14}C) and stable carbon isotopic ($\delta^{13}\text{C}$) data for the open mangrove site. Some values were not measured, indicated by N.M.

Interval	^{14}C Prep Method	Fm Reported	Fm Reported Error	Fm Blank Corrected	Fm Error Blank Corrected	$\mu\text{mol CO}_2$	$\delta^{13}\text{C}$ (‰)
DB-1722-2 UFU1A (13-14 cm) 1C	Ramped PyrOx	1.1458	0.0023	1.1521	0.0046	22.4	-29.57
DB-1722-3 UFU1A (13-14 cm) 1C	Ramped PyrOx	1.1456	0.0023	1.1515	0.0044	23.9	-29.16
DB-1722-4 UFU1A (13-14 cm) 1C	Ramped PyrOx	1.1401	0.0023	1.1462	0.0045	23.0	-28.82
DB-1722-5 UFU1A (13-14 cm) 1C	Ramped PyrOx	1.0918	0.0064	1.1270	0.0246	3.5	-28.07
DB-1724-1 UFU1A (16-17 cm) 2D	Ramped PyrOx	1.1277	0.0023	1.1387	0.0074	12.4	-28.86
DB-1724-2 UFU1A (16-17 cm) 2D	Ramped PyrOx	1.1339	0.0023	1.1399	0.0045	23.0	-29.42
DB-1724-3 UFU1A (16-17 cm) 2D	Ramped PyrOx	1.1402	0.0022	1.1458	0.0042	24.7	-29.12
DB-1724-4 UFU1A (16-17 cm) 2D	Ramped PyrOx	1.1346	0.0022	1.1401	0.0042	24.9	-28.88
DB-1724-5 UFU1A (16-17 cm) 2D	Ramped PyrOx	1.1065	0.0023	1.1160	0.0067	13.6	N.M.
DB-1725-1 UFU1A (24-25 cm) 2A2	Ramped PyrOx	1.0732	0.0025	1.0836	0.0076	11.5	-28.9
DB-1725-2 UFU1A (24-25 cm) 2A2	Ramped PyrOx	1.0730	0.0020	1.0790	0.0046	19.9	-29.4
DB-1725-3 UFU1A (24-25 cm) 2A2	Ramped PyrOx	1.0787	0.0033	1.0845	0.0052	20.8	-29.28
DB-1725-4 UFU1A (24-25 cm) 2A2	Ramped PyrOx	1.0744	0.0020	1.0788	0.0036	27.3	-29.11

Table 1E (Continued) Radiocarbon (^{14}C) and stable carbon isotopic ($\delta^{13}\text{C}$) data for the open mangrove site. Some values were not measured, indicated by N.M.

Interval	^{14}C Prep Method	Fm Reported	Fm Reported Error	Fm Blank Corrected	Fm Error Blank Corrected	$\mu\text{mol CO}_2$	$\delta^{13}\text{C}$ (‰)
DB-1725-5 UFU1A (24-25 cm) 2A2	Ramped PyrOx	1.0691	0.0021	1.0743	0.0042	22.8	-28.94
UFU1A (31-32 cm) A	Bulk	1.0340	0.0039	1.0407	0.0070	31.3	-26.93
UFU1A (54-55 cm) D	Bulk	0.9336	0.0020	0.9407	0.0078	21.4	-26.51
UFU1A (104-105 cm) C	Bulk	0.8515	0.0037	0.8582	0.1020	15.7	-25.83
UFU1A (164-165 cm) C	Bulk	0.7509	0.0029	0.7558	0.1400	9.9	-24.54

Table 2E Radiocarbon (^{14}C) and stable carbon isotopic ($\delta^{13}\text{C}$) data for the confined mangrove site. The open mangrove is synonymous with the CCB site code in this study. Some values were not measured, indicated by N.M.

Interval	^{14}C Prep Method	Fm Reported	Fm Reported Error	Fm Blank Corrected	Fm Error Blank Corrected	$\mu\text{mol CO}_2$	$\delta^{13}\text{C}$ (‰)
CCB2 (4-6 cm) D	Bulk	1.0887	0.0025	1.0945	0.0052	41.3	-27.39
DB-1788-1 CCB2 (12-13 cm) D	Ramped PyrOx	1.1543	0.0032	1.1700	0.0104	9.2	-28.86
DB-1788-2 CCB2 (12-13 cm) D	Ramped PyrOx	1.1586	0.0022	1.1699	0.0074	12.9	-27.75
DB-1788-3 CCB2 (12-13 cm) D	Ramped PyrOx	1.1651	0.0022	1.1765	0.0074	12.9	-28.54
DB-1788-4 CCB2 (12-13 cm) D	Ramped PyrOx	1.1733	0.0025	1.1803	0.0050	21.4	-28.51
DB-1788-5 CCB2 (12-13 cm) D	Ramped PyrOx	1.1752	0.0023	1.1823	0.0049	21.2	-28.34
DB-1788-6 CCB2 (12-13 cm) D	Ramped PyrOx	1.1655	0.0022	1.1720	0.0046	22.8	-27.84
DB-1789-1 CCB2 (15-16 cm) D	Ramped PyrOx	1.1256	0.0023	1.1381	0.0084	10.8	-28.27
DB-1789-2 CCB2 (15-16 cm) D	Ramped PyrOx	1.1400	0.0023	1.1479	0.0055	17.7	-28.13
DB-1789-3 CCB2 (15-16 cm) D	Ramped PyrOx	1.1368	0.0023	1.1468	0.0068	13.85	-28.68
DB-1789-4 CCB2 (15-16 cm) D	Ramped PyrOx	1.1425	0.0023	1.1493	0.0049	20.55	-29.40
DB-1789-5 CCB2 (15-16 cm) D	Ramped PyrOx	1.1360	0.0022	1.1440	0.0056	17.21	-28.30
DB-1790-1 CCB2 (17-18 cm) B	Ramped PyrOx	1.0799	0.0027	1.0892	0.0069	13.05	-28.71

Table 2E (Continued) Radiocarbon (^{14}C) and stable carbon isotopic ($\delta^{13}\text{C}$) data for the confined mangrove site. Some values were not measured, indicated by N.M.

Interval	^{14}C Prep Method	Fm Reported	Fm Reported Error	Fm Blank Corrected	Fm Error Blank Corrected	$\mu\text{mol CO}_2$	$\delta^{13}\text{C}$ (‰)
DB-1790-2 CCB2 (17-18 cm) B	Ramped PyrOx	1.0745	0.0034	1.0809	0.0056	18.67	N.M.
DB-1790-3 CCB2 (17-18 cm) B	Ramped PyrOx	1.0786	0.0024	1.0860	0.0056	16.25	-29.26
DB-1790-4 CCB2 (17-18 cm) B	Ramped PyrOx	1.0798	0.0021	1.0843	0.0037	27.02	-28.77
DB-1790-5 CCB2 (17-18 cm) B	Ramped PyrOx	1.0786	0.0024	1.0822	0.0034	33.84	-28.14
DB-1793-1 CCB2 (20-21 cm) D	Ramped PyrOx	1.0326	0.0027	1.0460	0.0102	7.98	N.M.
DB-1793-2 CCB2 (20-21 cm) D	Ramped PyrOx	1.0400	0.0200	1.0456	0.0045	19.55	N.M.
DB-1793-3 CCB2 (20-21 cm) D	Ramped PyrOx	1.0413	0.0023	1.0505	0.0071	11.86	-29.82
DB-1793-4 CCB2 (20-21 cm) D	Ramped PyrOx	1.0414	0.0024	1.0456	0.0039	26.14	-29.77
DB-1793-5 CCB2 (20-21 cm) D	Ramped PyrOx	1.0382	0.0021	1.0435	0.0044	20.30	-28.88
DB-1792-1 CCB2 (22-23 cm) C	Ramped PyrOx	1.0071	0.0033	1.0217	0.0118	6.75	-28.92
DB-1792-2 CCB2 (22-23 cm) C	Ramped PyrOx	1.0023	0.0020	1.0077	0.0047	18.04	-29.60
DB-1792-3 CCCB2 (22-23 cm) C	Ramped PyrOx	1.0102	0.0021	1.0172	0.0058	14.21	-29.53
DB-1792-4 CCB2 (22-23 cm) C	Ramped PyrOx	1.0077	0.0021	1.0142	0.0054	15.26	-28.57

Table 2E Continued Radiocarbon (^{14}C) and stable carbon isotopic ($\delta^{13}\text{C}$) data for the confined mangrove site. Some values were not measured, indicated by N.M.

Interval	^{14}C Prep Method	Fm Reported	Fm Reported Error	Fm Blank Corrected	Fm Error Blank Corrected	$\mu\text{mol CO}_2$	$\delta^{13}\text{C}$ (‰)
DB-1792-5 CCB2 (22-23 cm) C	Ramped PyrOx	1.0033	0.0022	1.0091	0.0050	16.78	-27.37
CCB1 (31-32 cm) B	Bulk	1.0754	0.0025	1.0804	0.0048	46.0	-26.89
CCB1 (41-42 cm) D	Bulk	0.9925	0.0019	0.9964	0.0041	47.3	-26.45
CCB1 (79-80 cm) A	Bulk	0.8908	0.0021	0.8955	0.0061	27.1	-25.35
CCB1 (119-120 cm) C	Bulk	0.7835	0.0019	0.7851	0.0039	41.1	-25.86